Quaternary Science Reviews 92 (2014) 140–154

Contents lists available at ScienceDirect

Quaternary Science Reviews

journal homepage: www.elsevier.com/locate/quascirev

Invited review

Late Quaternary evolution of sediment provenances in the Central Arctic Ocean: mineral assemblage, trace element composition and Nd and Pb isotope fingerprints of detrital fraction from the Northern Mendeleev Ridge

N. Fagel [a,*], C. Not [b,c], J. Gueibe [d], N. Mattielli [d], E. Bazhenova [e]

[a] UR. AGEs – Argiles, Géochimie et Environnement sédimentaires, Université de Liège, B-4000 Liège, Belgium
[b] GEOTOP, UQAM, Montréal, Canada
[c] Atmosphere and Ocean Research Institute, University of Tokyo, Kashiwanoha, Japan
[d] G-Time, Université Libre de Bruxelles, Belgium
[e] Alfred Wegener Institute for Polar and Marine Research, Bremerhaven, Germany

ARTICLE INFO

Article history:
Received 27 November 2012
Received in revised form
6 December 2013
Accepted 12 December 2013
Available online 17 January 2014

Keywords:
Arctic Ocean
Sediment
Mineral assemblage
Trace element composition
Radiogenic isotope
Late Quaternary
Paleoceanography

ABSTRACT

Mineral assemblage, trace element content and Nd and Pb isotope signatures were analysed on the fine fraction (<20 μm) of sedimentary records from the Northern Mendeleev Ridge in the Central Arctic Ocean. Our aim was to identify the detrital particle provenance and to interpret the changes over the past ~250 ka in the relative contribution of the different source-areas in relation to paleoenvironmental conditions. The clay mineral assemblage and the Nd and Pb isotope signatures depict systematic changes over the Late Quaternary. The bulk mineralogy exhibits increases in the relative contribution of carbonate minerals *vs.* silicates in interglacial/deglacial intervals. In glacial intervals, the mineral assemblage of the <20 μm fraction is characterised by an enrichment in kaolinite, counterbalanced by a decrease in illite. The Nd and Pb isotope signatures of <20 μm fraction are interpreted using a three end-member mixing model, involving crustal supplies from North America and Canada, from the Siberian margin and some from volcanic material. A compilation of geochemical signatures of geological terraines surrounding the Arctic Ocean allowed each end-member to be assigned a representative signature, averaging the signal of the eroded terraines. The Suspended Particulate Matter (SPM) of the MacKenzie River represents an average signature of the sedimentary supplies delivered from the North American platform and Canadian margin. The SPM of the Lena River reflects the mean sedimentary signature of the Siberian platform. The Okhotsh-Chukotka province from the Eastern border of Siberia is identified as the most probable volcanic source. Late Quaternary evolution of the estimated relative contribution of the three end-members confirms that the sediment provenances in the Central Arctic Ocean remain close to the current conditions during past interglacials/deglacials MIS1–3, MIS5/TII and MIS7/TIII. In contrast, glacial conditions (MIS4 and MIS6) record minimum supplies from the American margin, associated with increased volcanic contribution, to the Mendeleev Ridge core location suggesting a different sea-ice circulation associated with a low sea-level and reduced shelf area.

1. Introduction

During the last decade many oceanographical cruises and environmental studies have been performed in the Arctic (e.g., Darby et al., 2005; McDonald et al., 2005; Stein, 2008; Polyak et al., 2009; Jakobsson et al., 2010a) emphasising its sensitivity to climate change but also its influence on climate regulation (e.g., Kellogg, 1995) and on global thermohaline circulation (THC, e.g., Hoffman et al., 2013; Jang et al., 2013). Provenance studies in particular have allowed changes in surface Arctic circulation over the late Pleistocene to be determined. Petrography of ice-rafted detritus (IRD) has been used to identify the main sources of Arctic sediments (Bischof and Darby, 2007). In addition, the purely detrital origin of Arctic clays (Washner et al., 1999) allows their distribution in surface sediments to be used as a provenance indicator (Vogt et al., 2001; Visconsi-Shirley et al., 2003; Krylov et al., 2008; Vogt

* Corresponding author. Fax: +32 4 366 2029.
E-mail address: nathalie.fagel@ulg.ac.be (N. Fagel).

0277-3791/$ – see front matter © 2014 Elsevier Ltd. All rights reserved.
http://dx.doi.org/10.1016/j.quascirev.2013.12.011

and Knies, 2008; Stein et al., 2010). However, Darby et al. (2011) have suggested that sea ice clay mineral assemblages do not match specific sources, "making it difficult to use as a provenance tool by itself". Such mineralogical tracers are helpful, although sources are better constrained using additional tracers like sedimentary isotope signatures.

In the Arctic Ocean a few studies on radiogenic isotopes of Sr, Nd and Pb have been done on bulk sediments (Tütcken et al., 2002; Haley et al., 2008a), on the authigenic fraction of sediment obtained after leaching (Winter et al., 1997; Haley et al., 2008a, 2008b; Maccali et al., 2012; Haley and Polyak, 2013; Jang et al., 2013) and on detrital fractions (Winter et al., 1997; Asahara et al., 2012). Haley et al. (2008b) have investigated the variability of Arctic intermediate circulation over late Pleistocene glacial/interglacials using radiogenic isotope signature of leached sediments. For example, metal-coating extracted by leaching represents an authigenic signal; its isotope signature records a fingerprint of water. Their Lomonosov Ridge data showed pronounced Nd isotope variability on millennial time-scales over the past 500 ka. These variations are interpreted as switches between an interglacial modern-like circulation mode, and a glacial mode. During glacial periods, the circulation of Arctic Intermediate Waters (AIW) was controlled by enhanced input of shelf waters from brine sources (Kara Sea) together with a restricted input from the North Atlantic.

In this study we focus on the detrital sedimentary fraction as it brings information on particle provenance and indirect information on circulation (see Fagel, 2007 for a review). The implication for the transport agent will mainly concern surface circulation and sea-ice drifting. By coupling mineralogy and geochemistry of the fine sedimentary fraction (<20 μm) our aims are to (1) identify the detrital particle provenance in sediments from the Central Arctic Ocean; (2) to estimate the relative contribution of the different sources and; (3) to interpret the changes in the relative contribution of the different source-areas in terms of paleoenvironmental changes over the past ~250 ka in the Central Arctic Ocean.

2. Methods and study area

2.1. Sediment core description

Two sediment cores were collected at ~1600 m on the Mendeleev Ridge (Fig. 1) during the HOTRAX 2005 cruise (Darby et al., 2005). Here we present results from the multicore HLY0503-12MC8 (12 MC, 83°17.797′ N, 171°54.994′ W, 1586 m water depth). Note all results from the upper part (down to 78 cm) of the trigger weight core HLY0503-12TC (12TC, 83° 17.465′ N, 171° 57.464′ W, 1585 m water depth) are reported as Supplementary material. The sediment consists of alternating layers of yellow-brown clayey sands and dark brown sandy clays and clays (description from L. Polyak, comm. pers. – Fig. SM1). Such lithology is common in Arctic Ocean sediments: sandy layers are deposited during glacial intervals, and clayey layers are deposited during interglacials (e.g., Jakobsson et al., 2000; Polyak et al., 2004). Some centimetric sandy layers attributed to IRD are scattered through the cores. In particular two

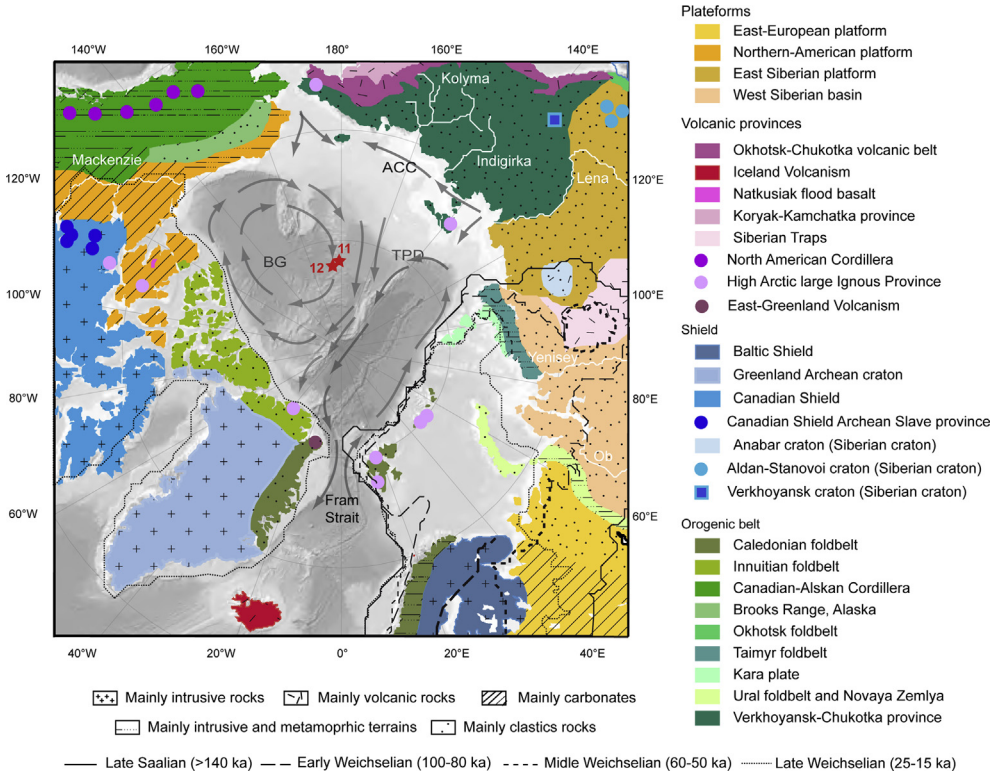

Fig. 1. Map of coring site locations 11 and 12 (Darby et al., 2005) and surface current distribution (Aagaard, 1989). The coring site is currently influenced by the two main Arctic surface currents – the Beaufort Gyre (BG) and the Transpolar Drift (TPD). The Arctic Ocean is highly stratified and consists of three water masses: the surface waters (<250 m), the intermediate waters (250–1700 m) and the deep waters (>1700 m). The surface waters consist of the low saline Polar Mixed Layer (PML) down to ~50 m and the more saline halocline layer (Schlosser et al., 1995; Sellen et al., 2010). At the moment, the BG mainly controls the oceanic and sea-ice circulation in the Amerasian Basin whereas the TPD is efficient in the Eurasian Basin of the Arctic Ocean. The modern front between the BG and the TPD is close to the Lomonosov Ridge (e.g., Aagaard et al., 1985; Rudels et al., 2012) but its location may have changed over time, influenced in particular by the Arctic Oscillation Index (Macdonald et al., 2005). All intermediate and deep waters flow along an anticlockwise gyre through the basins (Rudels et al., 2012). Schematic structural map showing the distribution and the main lithology of the different terraines adjacent to the Arctic Ocean (AMAP, 1998; Cocks and Torsvik, 2007; Harrison et al., 2008; Tikhomirov et al., 2008; http://atlas.nrcan.gc.ca). Main structural units are identified by colour: shield in blue, orogenic foldbelt in green, sedimentary platform in yellow and volcanic province in pink. Maximum limit of the Eurasian and Amerasian Ice Sheet during the late Quaternary are respectively from Svendsen et al. (2004) and Dyke et al. (2002), updated in accordance with England et al. (2009). BG, Beaufort Gyre; TPD, Transpolar Drift.

sandy sediment layers with pink clasts are observed at 6 cm and 58–61 cm in 12TC core (see Fig. SM1). The coring site is currently influenced by the two main Arctic surface currents – the Beaufort Gyre (BG) and the Transpolar Drift (TPD).

2.2. Sediment stratigraphy

The establishment of chronostratigraphies for sediment cores from the Arctic Ocean (and especially from the Central Arctic Ocean) is far from being straightforward (Fig. 2). For example, during the last climatic cycle, uncertainties persist both with determining reservoir corrections for ^{14}C ages, and on the influence of brine on oxygen isotope composition of foraminifera. Initially, we attempt to establish the required chronology using ^{18}O and ^{13}C isotopic composition and ^{14}C ages on planktic foraminifera in a closely located core, HLY0503-11MC8. However, based on these data the chronology obtained was limited (see Not and Hillaire-Marcel, 2010 for details). For this reason, we use non-traditional methods including U-series isotopes and especially the particle reactive isotope ^{230}Th to add time constraints as described in Not and Hillaire-Marcel (2010). The ^{230}Th profile in core 12MC is characterised by two distinct regimes, one with very low ^{230}Th values suggesting an absence of scavenging or more probably an export of the ^{230}Th produced in the water column, and a second regime with higher ^{230}Th values suggesting an efficient scavenging of the ^{230}Th produced in the water column. In the latter regime, assuming no lateral input of ^{230}Th, the decrease in excess ^{230}Th in the sediment is only a function of the time since the settling of ^{230}Th in the sediment. From this hypothesis we can estimate the time elapsed between different layers. In core 12MC ~145 ka occurred between 2 cm and 18 cm, and 52 ka between 18 cm and 28 cm (see Fig. 6 in Not and Hillaire-Marcel, 2010). In this context, periods with higher ^{230}Th activities suggest higher particle fluxes linked to enhanced sea-ice circulation during warmer periods such as an interglacial or more probably a period of deglaciation or an interstadial in the Arctic Ocean. Given this, the first 8 cm should be related to Marine Isotope Stage (MIS)3, as MIS1, the interglacial sedimentation *sensu-stricto* is restricted to the first centimetre of the core (see ^{14}C of ~8500 y at 0.5 cm of 11MC) (Not and Hillaire-Marcel, 2010). The layer between 17 cm and 21 cm corresponds to interstadials during MIS5, while the layer that starts at 26 cm corresponds to the deglaciation of MIS8 or to the beginning of MIS7. Periods with lower ^{230}Th activity correspond to periods with limited scavenging, possibly related to an active ice margin or the development of sea ice production during a period of extended ice sheet presence. Full glacial conditions are most likely not recorded in the sediment core, as shown for the Last Glacial Maximum (LGM) in Mendeleev and Lomonosov Ridge (Not and Hillaire-Marcel, 2010, 2012) due to both the almost absence of sedimentation when thick pack-ice conditions persist and the slow sedimentation. However, while this method allows us to broadly add time constraints, we cannot use these constraints to determine the sedimentation rate since it does not take into account potential changes in the sedimentation rate, or even the absence of sedimentation, which are possibly important in the Arctic Ocean (e.g. during the LGM). Thus, it is difficult to validate a precise chronostratigraphy as most likely the glacial periods identified correspond to non constant and scarce sediment deposition, when ice margin or sea ice production are active and the interglacial/deglacial periods identified correspond to events with significant freshwater flow and sea ice circulation. For these reasons, all the data shown in this study are shown on a depth scale not a time scale. Also, we used MIS as benchmarks and thus it is not possible to estimate any sedimentation rate (Fig. 2 and Supplementary material). Details methodological information for inorganic carbon content, ^{210}Pb and ^{230}Th analyses can be found in Not and Hillaire-Marcel (2010).

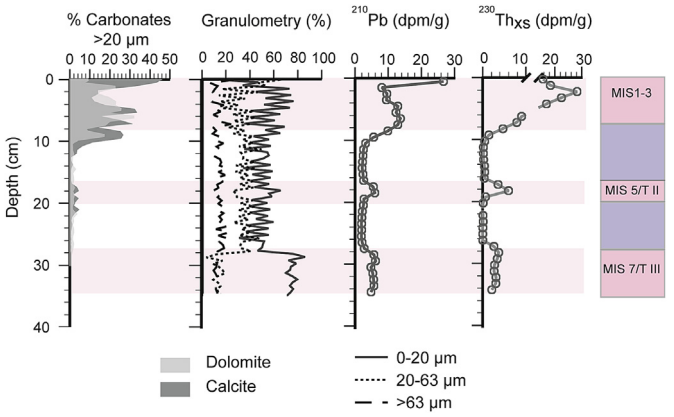

Fig. 2. Core description and stratigraphy. Carbonate content in fraction >20 µm, grain size distribution, ^{210}Pb and ^{230}Th$_{xs}$ data for 12MC core are from Not and Hillaire-Marcel (2010). The scale on the right gives the tentative positions of the Marine Isotopic Stages (MIS), as defined by Martinson et al. (1987). Note that the carbonate content of the MC is provided only for the first 24 cm.

2.3. Regional geology

The geology of outcropping terraines adjacent to the Arctic Ocean is quite complex. Fig. 1 proposes a schematic structural map showing the distribution and the main lithologies of the different terraines. We identify 4 structural units: shield, orogenic foldbelt, sedimentary platform and volcanic province (sources: AMAP, 1998; Cocks et Torsvik, 2007; Harrison et al., 2008; Tikhomirov et al., 2008; http://atlas.nrcan.gc.ca).

The older crustal terraines, mainly made by Archean or Proterozoic magmatic (plutonic) and metamorphic rocks, are the Greenland Archean Craton, the Canadian Shield, the Siberian Craton and the Baltic Shield.

On the North American side, the main orogenic foldbelts (mainly metamorphic terranes) are the Greenland Caledonian crust, the North Greenland Innutian crust and the North America Cordillera. On the Eurasian side, 4 foldbelts are recognised, i.e., Verkhoyansk-Chukotka province, the Kara Plate and Tamyr foldbelt, the Ural and Novaya Zemlya foldbelt and the Scandinavian Panafrican crust.

The main North American sedimentary platform is carbonate-rich (Phillips and Grantz, 2001), and mainly drained by the MacKenzie River. In addition, the Sverdrup Basin of the Canadian Arctic Islands (North Greenland, Ellesmere Island and Canadian Arctic Archipelago) constitutes the Paleozoic and Mesozoic sedimentary cover of the Canadian Shield, made by sand and fine-grained terrigenous material (shale or mudstone, Patchett et al., 2004). The Siberian platform is composed by Precambrian and Cambrian limestones, Jurassic to Cretaceous terrigenous sediments and Quaternary alluvial material (Rachold, 1999; Stein, 2008). The West Siberian Basin and East European platforms are mainly composed by terrigenous sediment with some limestones.

The main regional Volcanic Provinces comprise continental flood basalts from North Greenland Proterozoic, High Arctic-Large Igneous Province (HALIP) (Buchan and Ernst, 2006) and the Permian and Triassic volcanic rocks of Siberian traps, intraplate volcanism of North American Cordillera, Bering Sea basalt province, Okhotsk-Chukotka province, and the convergent margins of the Pacific Aleutian and the Koryak-Kamchatka arcs. The Cretaceous volcanic rocks, dykes and sills of HALIP are widespread on Arctic margins, occurring on North Greenland (Cap Kane), on Ellesmere

Island and the Canadian Arctic Achipelago (Coronation Gulf), on Victoria island (Natkusiak flood basalt), Chukchi Peninsula, Novaya Zemylya, Svalbard and Franz Joseph islands (Fig. 1).

3. Methods

3.1. Mineral assemblage

Mineral assemblages were measured on the upper 80 cm of core 12TC (10 mm–20 mm resolution) and on the upper 34 cm of 12MC (5 mm resolution, analyses by Michel Preda, GEOTOP). Measurements were performed on a Siemens D5000 apparatus with a Cu Ka radiation, 2 mm divergence and antiscatter slits under 40 kV and 30 mA operating conditions. The XRD patterns were recorded by a Sol-X detector (detector slit 0.2 mm) between 2° and 45° 2θ using a step scan 0.02° and a step time of 0.6 s.

Samples were sieved at 63 μm and 20 μm. The bulk mineral assemblage of the sandy (>63 μm) and coarse silt (20–63 μm) fractions were analysed using X-Ray Diffraction (XRD) on random powder. Mineral abundance is based on the height of diagnostic peaks multiplied by a corrective factor (Cook et al., 1975). The accuracy was estimated ±10%.

The clay mineral assemblage was identified on oriented aggregates (Moore and Reynolds, 1997) on both the <20 μm and the clay <2 μm fractions. The clay fraction was extracted from the <20 μm fraction by sedimentation, after a settling time calculated from the Stoke's law. The clay fraction was treated with HCl 0.1 N to remove the calcite. Routine XRD clay analyses included the successive measurement of an X-ray pattern in air-dried or natural condition (N, between 2° and 30° 2θ), after solvation with ethylene glycol for 24 h (EG, between 2° and 15° 2θ), and after heating to 500 °C for 4 h (500, between 2° and 15° 2θ). Semi-quantitative estimations (±5–10%) of the main clay mineral groups (illite *s.l.* for true mica group, chlorite, smectite, kaolinite *s.l.* for serpentine – kaolin group, according to Martin et al., 1991) was based on the height of diagnostic peaks measured on EG runs, i.e. at 7Å for kaolinite, 10Å for illite and 14Å for chlorite. The occurrence of kaolinite is deduced from a double peak around 3.5 Å, resulting from the partial overlapping of the (004) chlorite reflection at 3.54 Å and the (002) kaolinite reflection at 3.57 Å under either N or EG conditions (Elverhøi and Rønningsland, 1978). The chlorite/kaolinite peak intensity ratio measured at 3.54–3.57 Å is then applied to the intensity of the 7 Å (EG) peak to estimate the contribution of kaolinite. The smectite content was deduced by its collapse at 10Å after heating. Each diagnostic peak was multiplied by a corrective factor (0.7 for kaolinite, 1 for illite and smectite, 0. 4 for chlorite – Boski et al., 1998) and values were summed up to 100%. More details are given in Fagel and Boës (2008). In parallel, the clay mineral assemblage was also determined using the Macdiff 4.2.5 software, designed by R. Petschick, University of Frankfurt, unpublished – (http://servermac.geologie.uni-frankfurt.de/Staff/Homepages/Petschick/RainerE.html) (for details see Petschick et al., 1996). Macdiff determines the clay abundance from the area of diagnostic peaks multiplied by a corrective factor as defined by Biscaye (1965). Note the two methods give similar mineralogical trends even though absolute mineral abundance may be different (see Supplementary material for a comparison).

3.2. Trace element and isotope composition

The trace element content and Nd and Pb radiogenic composition of the sediment were measured by ICP-MS and MC-ICP-MS on the <20 μm fraction of core HLY0503-12MC. We retained the fine fraction as it was less sensitive to winnowing than the coarser fraction (Fagel et al., 2002). However, the selection of a specific size fraction requires special attention for further geochemical interpretations. Working on the <20 μm will (i) underestimate the ice streaming and glacial sediment contribution, especially silicates; (ii) underestimate the flux of materials coming form the ice production such as IRD; and (iii) overestimate the sedimentary pulse signature such as meltwater events. Note that the <20 μm fraction dominates in the MIS1–3, MIS5/TII and MIS7/TIII intervals (70–80% of the sediment) and it represents 50% of the sediment in MIS4 and MIS6 intervals.

For trace element content, samples prepared at ULB were first calcinated at 550 °C to remove organic content. After calcination, the samples were treated with HCl 0.1 N to remove any authigenic fraction and were then digested by a classical tri-acid attack HF–HNO_3–HCl in a laminar flow hood. Thirty seven trace elements (Li, Sc, Ti, V, Cr, Co, Ni, Cu, Zn, As, Rb, Sr, Y, Zr, Nb, Cd, Cs, Ba, Rare Earth Element or REE, Hf, Ta, Tl, Pb, Th and U) were measured by ICP-MS at the University Joseph Fourier of Grenoble (Table 1). Measurements of 4 international geostandards BR, BHVO, JSd1, JSd2 allowed precision estimates better than 5% at 2σ level.

Nd and Pb composition of the sediment were analysed by MC–ICP-MS on the <20 μm fraction of core HLY0503-12MC. The analytical protocol was defined according to Weis et al. (2006). Pb was isolated using an AG1-X8 anion exchange resin in HBr environment. The REE were purified by using an AG50-X8 cation exchange resin in HCl environment. Then Nd was eluted by using HDEHP-coated Teflon powder as the ion exchange medium also in an HCl environment.

The Pb and Nd isotopes were measured on a Nu Plasma MC-ICP-MS instrument (ULB, Belgium). The analyses were performed by static multicollection in wet (Pb) or dry (Nd) mode. For Pb, measurements were corrected 1) for mass fractionation by using Tl as an internal standard then; 2) for instrumental drift by applying the sample standard bracketing method using NBS981 standard solution. Note repeated measurements of the NBS981 standard ($n = 41$) gave $^{208}Pb/^{204}Pb$ (36.7139 ± 0.0020), $^{207}Pb/^{204}Pb$ (15.4967 ± 0.0008), and $^{206}Pb/^{204}Pb$ (16.9407 ± 0.0008)values, which are consistent with the long term laboratory values ($^{208}Pb/^{204}Pb$ 36.7156 ± 89, $^{207}Pb/^{204}Pb$ 15.4970 ± 26, $^{206}Pb/^{204}Pb$ 16.9405 ± 37, $n = 1628$) and with the recommended values (Galer and Abouchami, 1998; Abouchami et al., 2000). Three replicates and three duplicates confirm the good reproducibility values of the measurements and the representativity of the sample sets (Table 2). Total blanks were negligible (≤10 pg). For Nd, measured $^{143}Nd/^{144}Nd$ ratios were corrected 1) for mass fractionation using the $^{146}Nd/^{144}Nd$ values; then 2) for instrumental drift by sample standard bracketing relative to the Rennes standard (Chauvel and Blichert-Toft, 2001). Repeated Rennes standard measurements (0.511952 ± 0.000007, $n = 17$) are consistent with the value obtained by Chauvel and Blichert-Toft (2001). Total blank is negligible (8 pg). One replicate attests the good reproducibility of the measurements. The εNd was defined as follows: $\varepsilon Nd = [((^{143}Nd/^{144}Nd)_{sample} - 0.512638))/0.512638] \times 10{,}000$ with 0.512638 as the CHUR composition (data from Wasserburg et al., 1981).

4. Results

4.1. Mineral assemblage

The bulk mineral assemblage depicts pronounced changes in the relative contribution of carbonates (2% < calcite < 60%, 2% < dolomite < 30%) with regard to silicates (see Supplementary material for a comparison between MC12 and TC12). In core 12MC a first carbonate-rich layer (0–8 cm) is observed during MIS1–3 and a second, less marked, coincides with MIS5/TII (Fig. 2). In core 12MC

Table 1
Trace element data of the 12MC cores measured by ICP-MS on the fine <20 μm sedimentary fraction. Data are given in ppm. D = duplicate analyses, R = replicate analyses. A mean value has been assigned for each lithology, calculated from the elemental composition of the silicate-rich or the carbonate-rich samples.

Sample interval cm	0	2	4	6	30	32	34	10	12	15	15D	17	17D	17R	18	19	22	22R	25	27	Mean carbonate	Mean silicate
	0–0.5	2–2.5	4–4.5	6–6.5	30–30.5	32–32.5	34–34.5	10–10.5	12–12.5	15–15.5		17–17.5			18–18.5	19–19.5	22–22.5		25–25.5	27–27.5		
Li	68.3	71.3	61.6	47.7	64	62.9	65.8	82.1	75.6	70	73	66	60.1	61.1	70.4	61.4	63.1	60.5	50.1	57.1	**63.1**	**66.2**
Sc	16.1	17	15.1	12.3	17.9	17.2	17.4	19.3	19.6	19	17.6	19.8	19.4	19.3	19.4	17.5	18.8	19.2	13.4	14.4	**16.1**	**17.9**
Ti	4559	4789	4385	3438	4812	4847	5006	5964	6063	5633	5854	5723	5604	5688	5462	5729	6045	6206	5763	5386	**4548**	**5752**
V	210	193	168	145	193	179	196	237	239	240	248	202	195	201	211	229	218	222	207	201	**183**	**220**
Cr	96.8	96.1	85.6	69.8	99	96.7	100	120	132	116	119	107	107	109	103	113	115	116	105	101	**92.0**	**112**
Co	172	169	105	98.8	95.8	110	130	36.1	21.9	22.9	23.5	79.7	77.4	79.4	102	30.5	29.8	29.6	19.4	68.3	**126**	**45.6**
Ni	148	137	123	143	100	125	145	68.2	67	52.5	54.3	69.8	67.6	68.9	100	63.5	52.2	52.5	45.3	68.6	**132**	**65.2**
Cu	93.6	91.5	81.4	69.4	85.4	86.5	101	54.3	43.9	85.5	49.8	68.4	66.2	68.5	76.9	56	41.8	41.9	39.6	59.4	**87.0**	**58.4**
Zn	140	152	129	108	147	136	150	142	138	157	135	144	142	147	152	136	126	128	117	125	**137**	**137**
As	50.1	49.1	45.4	38.5	40.5	40.9	46	69.1	69.7	81.4	79.2	52.8	52.4	52.6	58	66.4	62.5	61.9	58.7	55.2	**44.4**	**63.8**
Rb	127	127	112	85.1	131	116	131	108	111	115	107	116	119	120	117	110	107	106	107	112	**118**	**111**
Sr	210	191	208	281	165	158	176	171	164	179	177	201	187	196	171	174	176	176	170	178	**198**	**176**
Y	33.1	35.1	35.1	29	35.8	33.1	37.5	34.8	37	36.5	27	36.2	35.9	36.6	33	32	35.7	36	24	32.9	**34.1**	**33.6**
Zr	172	197	184	131	200	189	206	232	259	241	233	229	217	224	213	234	275	275	237	233	**183**	**239**
Nb	15.4	16.9	13.7	10.1	14.8	14.6	15.9	15.6	16.3	15.5	15	16.6	17.2	16.4	15.5	15.7	16.5	16.2	15.8	16.1	**14.5**	**16.0**
Cd	0.16	0.14	0.18	0.35	0.10	0.12	0.15	0.09	0.09	0.09	0.08	0.13	0.12	0.12	0.12	0.09	0.09	0.09	0.08	0.09	**0.17**	**0.10**
Cs	8.41	8.25	7.04	5.42	9.05	7.67	8.48	6.31	6.61	6.26	6.32	7.06	7.32	7.03	7.33	6.28	6.2	6.08	5.83	6.97	**7.76**	**6.54**
Ba	652	553	511	425	592	558	624	546	536	518	501	541	540	550	519	523	525	532	504	552	**559**	**529**
La	38	42.7	38.8	28.8	40.2	38.1	41.9	39.9	41.9	42.4	39.8	42.4	43.4	41.7	40.1	39.4	43.1	41.8	37.6	41.1	**38.4**	**40.9**
Ce	90.3	125	91.6	68.3	106	109	114	86.5	89.3	89.1	82.6	115	117	113	115	87.6	91	87.6	78.9	105	**101**	**95**
Pr	8.83	10.1	9.07	6.66	9.51	9.16	9.91	9.91	10.2	10	9.42	10.1	9.96	9.9	9.57	9.41	9.95	10.2	8.49	9.68	**9.03**	**9.70**
Nd	33.9	37.9	33	24	35.8	33.7	37.8	36.8	37.4	37.7	35.2	36.9	38	36.9	35.7	35	38.3	37.6	31.1	37.5	**33.7**	**36.3**
Sm	6.66	7.42	6.57	4.82	7.19	6.83	7.42	7.17	7.33	7.71	6.42	7.16	7.37	7.12	6.9	6.65	7	7.35	5.86	7.07	**6.70**	**6.98**
Eu	1.43	1.49	1.4	0.99	1.5	1.45	1.55	1.54	1.53	1.65	1.36	1.54	1.56	1.5	1.43	1.43	1.56	1.49	1.18	1.44	**1.40**	**1.48**
Gd	5.73	6.26	5.97	4.39	6.17	5.96	6.44	5.8	5.99	6.1	5.17	6.06	6.12	6.11	5.63	5.43	5.91	6.01	4.52	5.91	**5.85**	**5.71**
Tb	0.92	1.03	0.91	0.73	1.00	0.95	1.03	0.97	0.97	1.01	0.80	0.97	0.98	0.99	0.93	0.86	0.95	0.97	0.71	0.94	**0.94**	**0.92**
Dy	5.41	5.55	5.56	4.15	5.63	5.62	5.97	5.64	5.71	5.73	4.77	5.7	5.8	5.56	5.47	5.08	5.6	5.47	3.88	5.41	**5.41**	**5.36**
Ho	1.1	1.16	1.11	0.91	1.16	1.15	1.26	1.18	1.17	1.16	0.92	1.18	1.17	1.19	1.09	1.02	1.12	1.15	0.79	1.09	**1.12**	**1.09**
Er	3.08	3.31	3.26	2.59	3.35	3.24	3.69	3.29	3.4	3.27	2.55	3.45	3.38	3.42	3.18	2.97	3.28	3.35	2.25	3.16	**3.22**	**3.14**
Yb	2.93	3.13	3	2.49	3.11	3.12	3.47	3.2	3.22	3.09	2.4	3.19	3.16	3.18	3.03	2.82	3.16	3.17	2.09	2.96	**3.04**	**2.97**
Lu	0.46	0.47	0.45	0.39	0.49	0.48	0.52	0.48	0.50	0.48	0.37	0.49	0.50	0.50	0.46	0.43	0.48	0.49	0.32	0.46	**0.46**	**0.46**
Hf	4.45	4.96	4.31	3.26	4.89	4.67	5.2	5.57	6.12	5.61	5.63	5.59	5.58	5.57	5.35	5.67	6.39	6.46	5.68	5.81	**4.53**	**5.75**
Ta	0.94	1.0	0.71	0.46	0.97	0.91	1.0	1.03	0.93	0.85	0.97	1.04	1.07	1.1	0.97	1.0	1.03	1.05	1.01	1.01	**0.85**	**0.99**
Tl	2.09	1.22	1.15	1.31	1.3	1.25	1.63	1.38	1.57	1.1	1.11	1.43	1.4	1.41	1.33	1.19	0.95	0.95	0.93	1.28	**1.42**	**1.24**
Pb	30.2	31.3	26.1	21.7	29.1	28.7	31.7	22.1	20.3	21.3	20.3	25.7	25.6	26.5	42.4	21.2	19.1	19.5	18.3	23.8	**28.4**	**23.8**
Th	11.8	14.8	12	8.76	14.1	12.9	14	11.6	11.6	11.9	11.2	13.5	13.6	13.8	13.6	11.7	11.8	12	10.2	12.4	**12.6**	**12.0**
U	2.76	2.79	2.53	2.24	2.69	2.44	2.84	2.92	3.17	2.74	2.75	2.5	2.56	2.62	2.47	2.43	2.58	2.62	2.29	2.56	**2.61**	**2.63**

Table 2
Nd and Pb isotope data of 12MC core measured on fine <20 μm calcite-free sedimentary fraction by MC–ICP-MS. Underlined values correspond to duplicate analyses.

Sample	Interval cm	$^{143}Nd/^{144}Nd$	2σ	εNd	$^{208}Pb/^{204}Pb$	2σ	$^{207}Pb/^{204}Pb$	2σ	$^{206}Pb/^{204}Pb$	2σ	$^{208}Pb/^{206}Pb$	2σ	$^{207}Pb/^{206}Pb$	2σ
Carbonate-rich layers														
0	0-0.5	0.512099	0.000006	−10.5	38.7584	0.0017	15.6034	0.0006	18.8033	0.0006	2.0613	0.00004	0.8298	0.00001
	0-0.5D	0.512080	0.000007	−10.9										
2	2-2.5	0.512009	0.000010	−12.3	39.0093	0.0019	15.6325	0.0008	18.9994	0.0009	2.0532	0.00005	0.8228	0.00001
	2-2.5D				39.0300	0.0017	15.6333	0.0008	19.0107	0.0009	2.0531	0.00004	0.8223	0.00001
4	4-4,5	0.512029	0.000007	−11.9	38.9915	0.0021	15.6326	0.0009	19.0081	0.0011	2.0514	0.00005	0.8224	0.00001
	4-4,5D				39.0045	0.0026	15.6372	0.0011	19.0118	0.0012	2.0516	0.00005	0.8225	0.00002
	4-4.5Dbis				39.0137	0.0018	15.6357	0.0007	19.0202	0.0008	2.0512	0.00004	0.8221	0.00001
6	6-6.5	0.512083	0.000006	−10.8	38.9286	0.0021	15.6314	0.0008	18.9861	0.0007	2.0504	0.00004	0.8233	0.00001
30	30-30.5	0.512134	0.000034	−9.8	38.9149	0.0030	15.6244	0.0011	18.9440	0.0014	2.0542	0.00007	0.8248	0.00002
34	34-34.5	0.512089	0.000007	−10.7	38.8691	0.0028	15.6180	0.0009	18.8859	0.0010	2.0581	0.00007	0.8270	0.00002
Silicate-rich layers														
8	8-8.5	0.512159	0.000008	−9.3	38.7838	0.0026	15.6122	0.0009	18.8476	0.0011	2.0577	0.00005	0.8283	0.00001
	8-8.5D	0.512155	0.000008	−9.4										
	8-8.5Dbis	0.512166	0.000008	−9.2										
10	10-10.5	0.512204	0.000006	−8.5	38.6224	0.0018	15.5829	0.0007	18.6991	0.0009	2.0654	0.00005	0.8333	0.00001
12	12-12.5	0.512231	0.000008	−7.9	38.6334	0.0021	15.5756	0.0007	18.7071	0.0008	2.0652	0.00005	0.8326	0.00001
12	12-12.5D				38.6426	0.0017	15.5791	0.0006	18.7109	0.0008	2.0652	0.00005	0.8326	0.00001
15	15-15.5	0.512185	0.000014	−8.8	38.6401	0.0023	15.5752	0.0008	18.6250	0.0009	2.0746	0.00004	0.8363	0.00001
16	16-16.5	0.512157	0.000105	−9.4	38.6363	0.0058	15.5722	0.0033	18.5863	0.0034	2.0790	0.00006	0.8378	0.00002
17	17-17.5	0.512108	0.000008	−10.3	38.8144	0.0028	15.6128	0.0010	18.8183	0.0010	2.0626	0.00005	0.8297	0.00002
17	17-17.5D				38.8441	0.0021	15.6144	0.0008	18.8349	0.0009	2.0623	0.00004	0.8290	0.00001
19	19-19.5	0.512122	0.000007	−10.1	38.6490	0.0016	15.5748	0.0006	18.5982	0.0008	2.0781	0.00005	0.8374	0.00001
20	20-20.5	0.512168	0.000037	−9.2	38.6248	0.0025	15.5767	0.0009	18.6283	0.0011	2.0735	0.00006	0.8362	0.00002
22	22-22.5	0.512125	0.000008	−10.0	38.5777	0.0019	15.5656	0.0007	18.4852	0.0009	2.0869	0.00005	0.8420	0.00001
25	25-25.5	0.512142	0.000007	−9.7	38.5584	0.0017	15.5602	0.0007	18.4875	0.0007	2.0856	0.00004	0.8417	0.00001
27	27-27.5	0.512122	0.000051	−10.1	38.7695	0.0026	15.5996	0.0010	18.7553	0.0013	2.0671	0.00005	0.8317	0.00001

the mineral assemblage of the sands (>63 μm) and coarse silts (20–63 μm) are composed of the same mineral assemblages (Fig. 3). Quartz, K-feldspars and plagioclase are the main silicates, with micas, pyroxene and amphibole as secondary minerals. In both cores, layers with punctual enrichments in amphibole (5–10%) are observed in the sandy fraction and/or in the coarse silty fraction (Fig. 3 and Supplementary material).

Quartz, feldspars, calcite and dolomite are still present in the finer sedimentary fraction (<20 μm). Due to the preferential orientation of the clay particles on the glass slide, only clay mineral assemblages have been estimated in the <20 μm and <2 μm fractions on the 12MC core (see Supplementary material for TC12 core data). Following the Biscaye's method, the mean clay mineral assemblages in MC12 is composed of 41% ± 10 of illite, 24% ± 6 of kaolinite, 22% ± 2 of chlorite and 12% ± 6 of smectite (Fig. 5). It is noticable that using a Biscaye-like calculation of the clay mineral group assemblage (Biscaye, 1965) increases the chlorite contents over the kaolinite content (see Supplementary material for details). Enrichments in kaolinite (≥30%), mainly counterbalanced by a decrease of illite, are observed in two intervals (10–16 cm and 23–26 cm in 12MC). According to the stratigraphy, those intervals correspond to glacial MIS4 and MIS6.

4.2. Trace element and isotope composition

The trace element composition of the <20 μm sediment fraction in core 12MC is reported in Table 1. Data normalised to primitive mantle (PM, data from Sun and McDonough, 1989) are reported as a spidergram (Fig. 4). The enrichment relative to PM, ranges between 100 and 300 for Cs, Rb, Th, U and Pb, between 10 and 100 for Nb, Ta, Ligth REE (LREE), Zr, Hf and Li, and between 4 and 8 for intermediate and heavy REE and Y. An averaged composition has been calculated for the silicate-rich and carbonate intervals (Table 1). Both patterns are similar. Carbonate-rich intervals are enriched in Sr whereas silicate-rich intervals are enriched in Zr and Hf. Shale-normalised data displays a flat REE pattern, slightly enriched (by factor of 1.3–1.7) relative to the crustal reference (data from

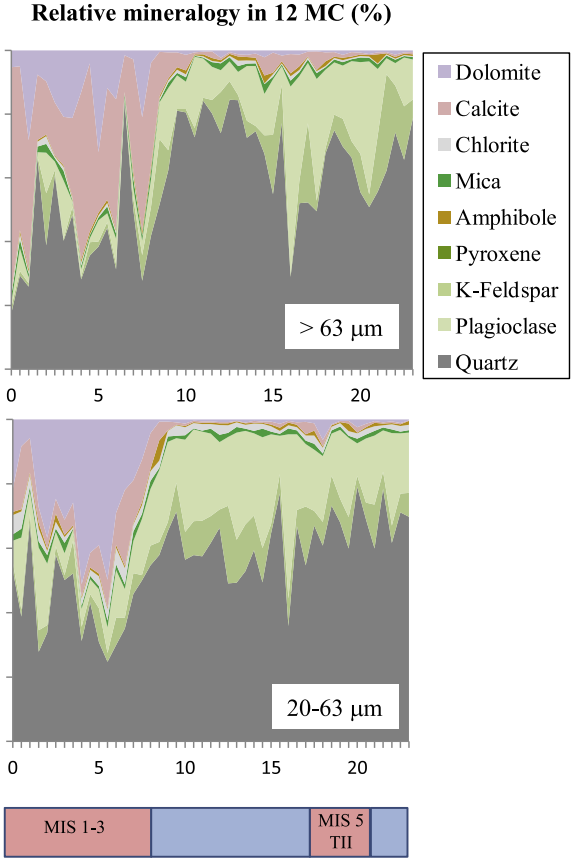

Fig. 3. Relative abundance (%) of main minerals identified by X-ray diffraction on bulk sediment powder on the coarse silt (20–63 μm, lower panels) and sandy (>63 μm, upper panels) fractions in 12MC core. Data are reported versus core depth in cm. The lower scales give the tentative position of the marine isotopic stages (MIS). Note that the mineralogical data of the MC are provided only for the first 24 cm.

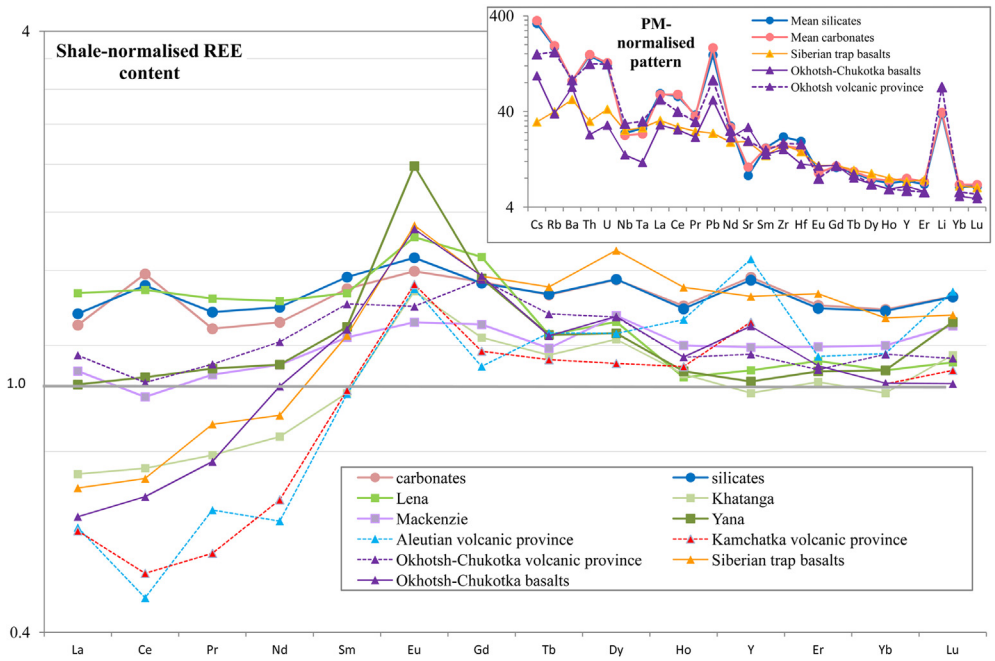

Fig. 4. Trace element composition measured on the fine <20 μm sedimentary fraction of 12MC core, Mendeleev Ridge (data from Table 1). Results have been normalised to shale values using the Upper Continental Crust data from McLennan (2001). Blue dot: silicate-rich sample; Pink dot: carbonate-rich sample. REE pattern of river suspended matter (SPM) are reported as squares: data for Lena, Kathanga and Yana from Rachold (1999); data from MacKenzie from Millot (2002) and Millot et al. (2003). Triangle, dashed line: Mean REE pattern of regional volcanic province are reported as triangles (data from GEOROC, 2003 database reported in Supplementary material). The upper panel presents the Primitive mantel-normalised trace element pattern of the two MC12 lithologies. The sediment signature is compared with the pattern of two volcanic provinces (i.e., Okhotsh-Chukotka and Siberian traps).

McLennan, 2001), with no significant differences between the two lithologies (Fig. 4).

The Nd and Pb isotope compositions show a large range of variations (Fig. 5): $-7.9 < \varepsilon Nd < -12.3$, $18.48 < {}^{206}Pb/{}^{204}Pb < 19.02$, $15.56 < {}^{207}Pb/{}^{204}Pb < 15.64$, $38.56 < {}^{208}Pb/{}^{204}Pb < 39.03$ (Table 2). Like the mineral assemblage of the fine fraction, the Nd and Pb signatures show systematically changes over silicate-rich and carbonate-rich intervals. All Pb ratios follow similar profiles with core depth. When εNd values are reported in parallel with the ^{207}Pb–^{206}Pb ratios (Fig. 5), as a general trend, the lower εNd values coincide with the lowest $^{207}Pb/^{206}Pb$ values. The shifts to lower εNd values are especially marked in the carbonate-rich intervals attributed to MIS1–3 and MIS5/TII.

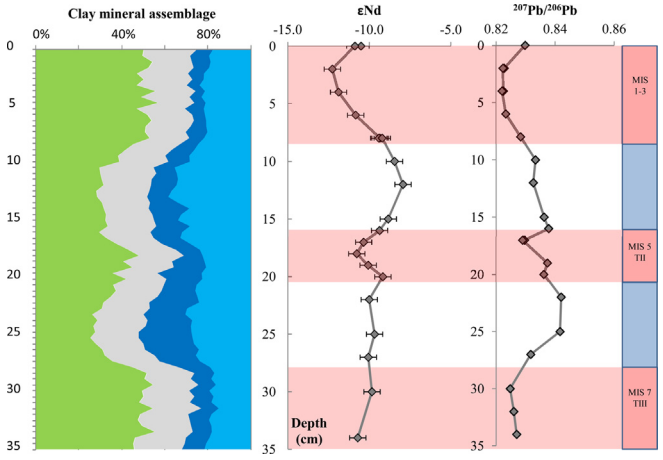

Fig. 5. Evolution of radiogenic isotope ratios versus core depth. $^{143}Nd/^{144}Nd$ (expressed as εNd ratio) and $^{207}Pb/^{206}Pb$ are measured on fine <20 μm calcite-free sedimentary fraction of 12MC core by MC–ICP-MS. Data from Table 2. Glacial/interglacial variability is observed in both isotopic ratios. More negative εNd and lower $^{207}Pb/^{206}Pb$ ratios are observed during interglacial periods MIS1–3, 5 and 7. The clay mineral assemblage of 12MC, as determined by the Biscaye's method (1965), is plotted in regard with the isotopic ratios. Note the enrichment in kaolinite and the relative depletion in illite in the glacial samples. The scale on the right gives the tentative position of the marine isotopic stages (MIS).

5. Discussion

The following discussion is divided into 4 sections. For identification of the sedimentary supplies to the Central Arctic Ocean we first characterise the geochemical signatures of the regional geology of outcropping terraines surrounding the Arctic Ocean. Second, we compare our sedimentary data with the signatures of the regional sources. Third, we define the regional sources and evaluate their relative contribution over glacial/interglacial within the sediment. Fourth, implications for the surface circulation in the Arctic Ocean are considered.

5.1. Characterisation of potential sedimentary sources

Based on a simplified geological map (Fig. 1), we have made for each regional source a compilation of (i) geochemical trace element composition (selected spidergrams or REE patterns plotted on Fig. 4; mean data listed in Supplementary material) and (ii) Nd and Pb isotope ratios of rocks (sample location, mean εNd and $^{206}Pb/^{204}Pb$ values reported on Fig.6; mean and median data listed in Table 3). The compilations are based on a literature review (all references are reported in table captions) and from the database GEOROC (2003). We have also taken into account the elemental and isotope composition of the suspended particle matter (SPM) from the main rivers draining the Arctic margins (Fig. 4). Detailed information on the characterisation of potential sedimentary sources is available in Supplementary material.

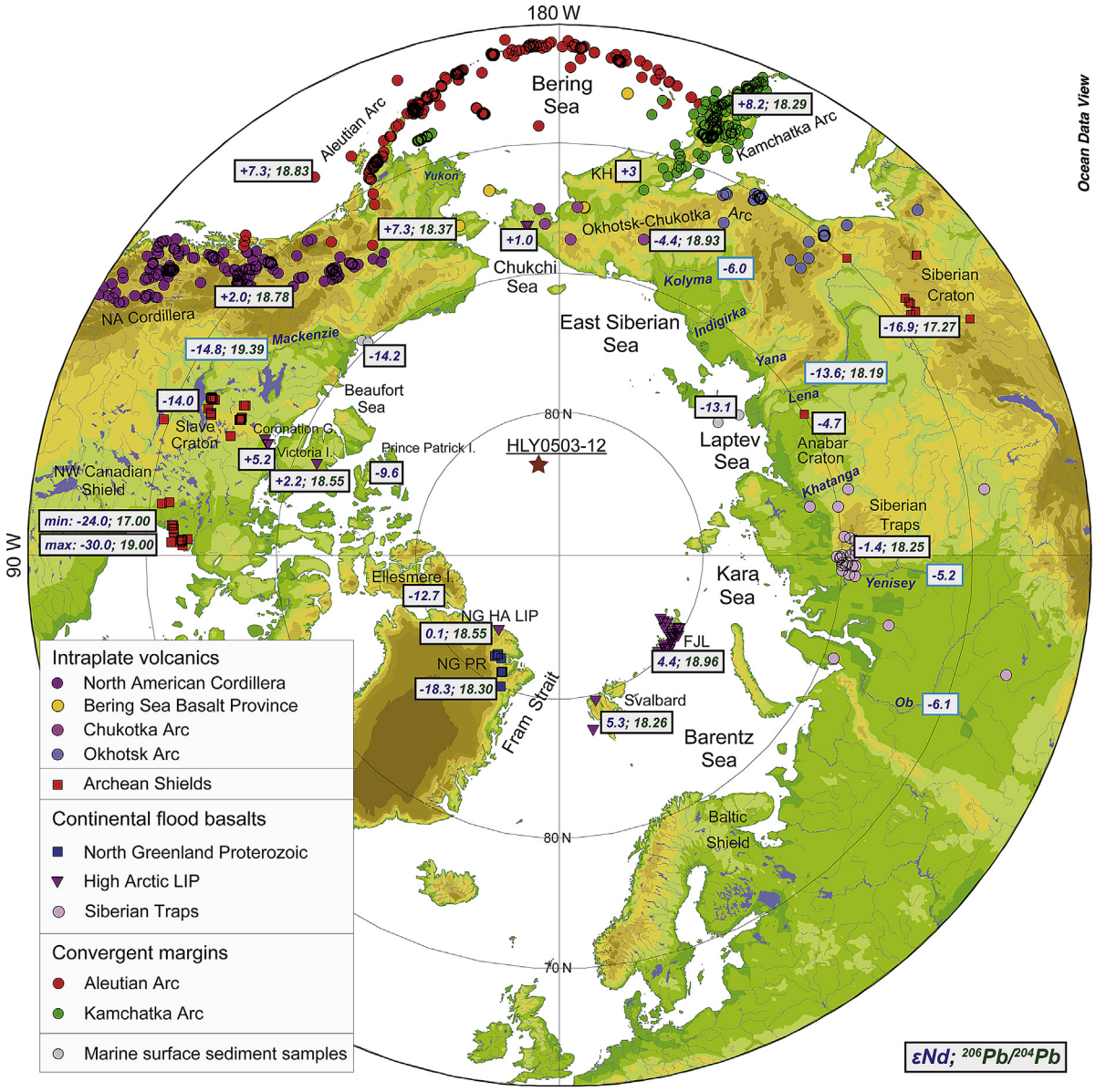

Fig. 6. Compilation of εNd and Pb isotope ratios of rocks, river SPM and surface sediments from the Arctic Ocean and surrounding terraines. Data for land-based rocks from different tectonic settings are compiled from the GEOROC database (GEOROC, 2003; and references therein) and from the literature (see references in table caption 3). Marine surface sediment values are from published data (Winter et al., 1997; Eisenhauer et al., 1999; Tütcken et al., 2002; Haley et al., 2008a; Asahara et al., 2012). River water data for Kolyma, Yenisey and Ob are from Zimmermann et al. (2009) and Porcelli et al. (2009). Values for the MacKenzie and Lena rivers suspended matter are from Millot et al. (2003). On the map, the first chiffer in the box corresponds to the εNd value, the second one to the $^{206}Pb/^{204}Pb$ ratio. Mean values are reported and/or minimum and maximum values. The map was drawn using the Ocean Data View.

5.2. *Identification of sedimentary supplies to the Central Arctic basin*

The Pb isotope compositions and the mineral assemblage of 12MC core (Table 2) support the sedimentary contributions from both American/Canadian and Eurasian margins to the Mendeleev Ridge sediment cores. In a $^{207}Pb/^{206}Pb$ vs. $^{208}Pb/^{206}Pb$ diagram, all 12MC samples define a linear trend ($r^2_{carbonate}$ = 0.99; $r^2_{silicate}$ = 0.88), consistent with a two-end-member mixing between SPM composition of MacKenzie and Lena (Fig. 7a). On one hand the carbonate-rich samples point towards the MacKenzie end-member with low $^{207}Pb/^{206}Pb$ and $^{208}Pb/^{206}Pb$ ratios. The mineral assemblages of the carbonate-rich layers highlight a contribution from the North American and/or Canadian margins to the Mendeleev Ridge sediment cores. Dolomite, in particular, is a mineral proxy for the MacKenzie river (Phillips and Grantz, 2001; Polyak et al., 2007, 2009; Stein et al., 2010) and the Canadian Arctic Archipelago (Krylov et al., 2008). Likely a kaolinite contribution ≥20% in 12MC core is also consistent with detrital supplies by massive iceberg discharge from the Canadian Arctic Archipelago (Darby, 1975; Krylov et al., 2008). Siberian shelf surface sediments are characterised by low kaolinite content (≤11%, Rossak et al., 1999; Washner et al., 1999; Visconsi-Shirley et al., 2003). Even observed in surface Arctic sediments from Franz Joseph Land or Barents (see surface clay mineral distribution map in Stein, 2008) kaolinite was only observed in significant proportion (25%) in ice dust from some North Canadian islands (Ellef Ringnes and Axel Heiberg islands - Darby et al., 2011).

Table 3
Characterisation of the regional sources classed by geographical sectors. Compilation of [Pb], [Nd] and Pb and Nd isotope ratios from literature and GEOROC (2003) database. Sources: (1) Dia Hantchi, 2000; (2) Revel et al., 1996; (3) Fagel et al., 2002; (4)Winter et al., 1997; (5) Tütcken et al., 2002; (6) Dupuy et al., 1995; (7) Millot et al., 2003; (8) Zimmermann et al., 2009; (9) Porcelli et al., 2009; (10) Tikhomirov et al., 2008; (11) Wooden et al., 1993; (12) Mühe et al., 1997; (13) Jicha et al., 2004; (14) Singer et al., 2007; (15). Patchett et al., 2004; (16) Goldstein et al., 1984.

Area	Source	Lithology	Variable	Nb.	208/204	207/204	206/204	208/206	207/206	[Pb]	[Nd]	[Sm]	eNd	Ref.
European margin	Baltic Shield	Craton				15.33	17.79		0.862				−18.0	1
European margin	Norway - Caledonian Crust (SPC)	Crust		19	38.25	15.60	18.45	2.07	0.846		25.0	4.3	−9.8	1,3
European margin	Svalbard	Crust		58							49.0		−14.6	5
European margin	Iceland	Volc.			38.03	15.46	18.44	2.06	0.838		12.0	3.8	8.1	1,2
European margin	Jan Mayen Seamounts	Volc.			38.60	15.51	18.82	2.05	0.824		36.0	7.0	6.0	1
European margin	HA LIP, Svalbard	Magm.	Mean	8	38.22	15.48	18.26	2.09	0.848	3.1	22.4	4.7	5.3	georoc
European margin	HA LIP, Franz Josef Land	Volc.	Mean	37	38.72	15.58	18.97	1.88	0.821	2.3	24.2	6.2	4.4	georoc
Greenland craton	Greenland Archean Craton (GAC)	Craton		11	35.65	14.74	14.91	2.43	1.003		25.0	3.7	−38.4	2,3
Greenland margin	East Greenland PanAfrican Crust (GPC)	Crust		3	38.90	15.59	18.60	2.09	0.839		25.0	4.7	−11.6	1-3
Greenland margin	N Greenl., Innutian fold belt (Proterozoic)	Crust	Mean	42	38.31	15.56	18.30	2.09	0.850	8.3	16.4	3.3	−18.3	georoc
Greenland margin	N Greenl., Innutian fold belt (Proterozoic)	Crust	Median	42	37.92	15.48	17.95						−16.4	georoc
Greenland margin	East Greenland	Basalts			38.26	15.50	18.42	2.08	0.841		27.5	6.1	2.0	1
Greenland margin	HA LIP, North Greenland Kap Kane	Volc.	Mean	17	39.13	15.53	18.55	2.11	0.837	15.4	58.3	9.1	0.1	georoc
Greenland margin	HA LIP, North Greenland Kap Kane	Volc.	Median	17	39.10	15.53	18.53						2.8	georoc
American margin	Brooks Range, Alaska	Crust	Min/max										−2/-11	4
American margin	Can. Cordillera, Cenozoic intraplate volc.	Volc.	Mean	186	38.51	15.59	19.05	2.02	0.818	13.1	36.6	7.0	2.0	georoc
American margin	Can. Cordillera, Cenozoic intraplate volc.	Volc.	Median	186	38.46	15.58	19.01						3.0	georoc
American margin	Can.Cordillera, Paleozoic intraplate volc.	Volc.	Mean	88	38.25	15.59	18.78	2.04	0.831	5.0	18.0	4.2	2.0	georoc
American margin	Can.Cordillera, Paleozoic intraplate volc.	Volc.	Median	88	38.12	15.58	18.66						2.6	georoc
American margin	Mackenzie River	SPM	Mean		39.17	15.67	19.39		0.808		28.0		−14.3	7,8,16
Canadian margin	NW Canadian Shield	Craton	Min/max				17/19						−24/-30	4
Canadian margin	Canadian Shield Archean Slave province	Craton	Mean	112						5.3	19.2	4.4	−14.0	georoc
Canadian margin	Canadian Shield Archean Slave province	Craton	Median	112									−12.3	georoc
Canadian margin	Canadian Archipelago St Patrick Island	Shale	Mean	24							30.5	5.7	−9.6	15
Canadian margin	Canadian Archipelago Central Ellesmere	Shale	Mean	25							33.1	6.3	−10.7	15
Canadian margin	Canadian Archipelago NE Ellesmere	Shale	Mean	9							30.2	5.5	−12.7	15
Canadian margin	HA LIP, Natkusiak flood basalt	magm.	Mean	9	38.71	15.55	18.55		0.839		10.6	3.3	2.2	6
Canadian margin	HA LIP, Natkusiak flood basalt	magm.	Median	9	38.79	15.56	18.65		0.834		10.5	3.1	2.4	6
Canadian margin	HA LIP, Natkusiak flood basalt	Magm.	Min	9	38.39	15.52	17.99		0.863				−4.0	6
Canadian margin	HA LIP, Natkusiak flood basalt	Magm.	Max	9	39.05	15.61	19.01		0.821				5.8	6
Canadian margin	HA LIP Coronation Gulf	Volc.	Mean	4							11.7	3.5	5.2	georoc
Canadian margin	HA LIP Coronation Gulf	Volc.	Median	4									3.8	georoc
Eurasian margin	Siberian craton, Aldan	Craton	Mean	16	37.47	15.38	17.27	2.17	0.891	12.3	28.0	5.7	−16.9	georoc
Eurasian margin	Siberian craton, Aldan	Craton	Median	16	37.47	15.38	17.27						−14.4	georoc
Eurasian margin	Siberian craton, Anabar	Craton	Mean	4							130	22.0	−4.7	georoc
Eurasian margin	Siberian craton, Anabar	Craton	Median	4									−4.7	georoc
Eurasian margin	Lena river	SPM			38.35	15.53	18.19		0.854		21.1		−13.6	7,9
Eurasian margin	Kolyma river	SPM											−6.0	9
Eurasian margin	Ob river	SPM											−6.1	9
Eurasian margin	Yenisey river	SPM											−5.2	9
Eurasian margin	Eurasian shelf sediments	Crust	Mean	31							21.0		−10.3	5
Eurasian margin	North-Central Siberia	Crust	Min/max				17/17.6						−10/-20	4
Eurasian margin	West Laptev Shelf	Crust	Mean	3									−9.4	5
Eurasian margin	East Laptev Shelf	Crust	Mean	3									−12.2	5
Eurasian margin	Novaya Zemlya - Shelf	Crust	Mean	6							22.0		−6.4	5
Eurasian margin	North-East Siberia	Crust	Min/max				18.1/18.9							4

Table 3 (*continued*)

Area	Source	Lithology	Variable	Nb.	208/204	207/204	206/204	208/206	207/206	[Pb]	[Nd]	[Sm]	eNd	Ref.
Eurasian margin	Siberian Traps	Basalt	Mean	20	38.18	15.51	18.38		0.844		17.4	4.1	−3.4	11
Eurasian margin	Siberian Traps	Basalt	Median	20	38.17	15.51	18.47		0.840		14.0	3.6	−3.1	11
Eurasian margin	Siberian Traps	Basalt	Mean	97	38.22	15.52	18.44	2.07	0.842	3.56	23.9	5.6	−2.1	georoc
Eurasian margin	Siberian Traps	Basalt	Median	97	38.20	15.52	18.50						−0.1	georoc
Eurasian margin	Siberian Traps	Volc.	Mean	280	37.93	15.33	18.25	2.08	0.840	5.26	44.0	7.6	−1.4	georoc
Eurasian margin	Siberian Traps	Volc.	Median	280	38.22	15.52	18.52						−0.7	georoc
Eurasian margin	Kamchatka Volcanic Province	Basalt	Mean	172	37.97	15.48	18.29	2.08	0.847	3.83	15.5	4.1	8.2	georoc
Eurasian margin	Kamchatka Volcanic Province	Basalt	Median	172	37.92	15.48	18.28						8.6	georoc
Eurasian margin	Kamchatka Volcanic Province	Volc.	Mean	362	37.94	15.48	18.27	2.08	0.847	6.14	17.3	4.5	8.2	georoc
Eurasian margin	Kamchatka Volcanic Province	Volc.	Median	362	37.975	15.50	18.3						8.6	georoc
Eurasian margin	Okhotsk-Chukotka volcanic belt	Basalt	Min	8	38.21	15.55	18.82		0.826		31.0	6.7	−5.0	10
Eurasian margin	Okhotsk-Chukotka volcanic belt	Basalt	Max	8	38.91	15.62	19.02		0.822		67.0	12.1	−3.6	10
Eurasian margin	Okhotsk-Chukotka volcanic belt	Basalt	Mean	8	38.70	15.60	18.93		0.824		46.1	8.6	−4.4	10
Eurasian margin	Okhotsk-Chukotka volcanic belt	Basalt	Median	8	38.78	15.61	18.95		0.824		41.0	7.8	−4.7	10
Eurasian margin	Okhotsh-Chutoka Volcanic Province	Volc.	Mean	54	38.11	15.47	18.30	2.08	0.845	12.8	31.6	6.3	−1.0	georoc
Eurasian margin	Okhotsh-Chutoka Volcanic Province	Volc.	Median	54	37.95	15.42	18.26						2.2	georoc
Eurasian margin	LIP, Chukchi Peninsula	Magm.	Mean	4						6.3	15.4	3.9	1.0	georoc
Eurasian margin	LIP, Chukchi Peninsula	Magm.	Median	4									0.9	georoc
Arctic Ocean	Gakkel ridge	Basalt			37.65	15.42	18.09		0.853		12.3	3.7	7	12
Pacific Ocean	Aleutian Arc	Basalt	Min		38.12	15.51	18.62		0.833		15.4	15.5	6.0	13,14
Pacific Ocean	Aleutian Arc	Basalt	Max		38.59	15.62	18.98		0.823		22.1	34.2	9.0	13,14
Pacific Ocean	Aleutian Arc	Basalt	Mean		38.37	15.56	18.83		0.826		11.2	4.8	7.3	13,14
Pacific Ocean	Aleutian Arc	Basalt	Median		38.40	15.57	18.85		0.826		9.7	3.2	7.3	13,14
Pacific Ocean	Aleutian Arc	Volc.			38.32	15.55	18.77	2.04	0.829	6.50	15.9	4.5	6.3	georoc
Pacific Ocean	Aleutian Arc	Basalt			38.41	15.57	18.85	2.04	0.826	4.8	14.5	4.7	7.2	georoc
Pacific Ocean	Bering Sea basalt province	Volc.	Mean	8	38.10	15.50	18.37	1.42	0.844		12.0	3.2	7.3	georoc
Pacific Ocean	Bering Sea basalt province	Volc.	Median	8	38.04	15.50	18.42						7.3	georoc

On the other hand in the $^{207}Pb/^{206}Pb$ vs. $^{208}Pb/^{206}Pb$ diagram the silicate-rich samples point towards the Lena end-member with more radiogenic $^{207}Pb/^{206}Pb$ and $^{208}Pb/^{206}Pb$ values. Punctual supplies from the Eurasian margin are consistent with spike occurrences of amphibole, a mineral proxy for East Siberian and Eastern Laptev seas (Krylov et al., 2008), probably related to IRD. Within the clay mineral assemblage the low averaged smectite content ($\leq$12%) in 12MC core agrees with Siberian supplies and discounts contributions from the smectite-rich Western Laptev and the Chukchi seas (Washner et al., 1999; Schoster et al., 2000; Visconsi-Shirley et al., 2003).

In a εNd-$^{207}Pb/^{206}Pb$ diagram (Fig. 7b) the 12MC signatures point towards an additional end-member characterised by less negative εNd values than the Mackenzie and Lena SPM. Among the numerous volcanic provinces surrounding the Arctic Ocean (Fig. 1) the volcanic Okhotsh-Chukotka province is retained as the most probable candidate since the Okhotsh-Chukotka and the Siberian Traps are characterised by the εNd values closer to the isotopic composition of MC12 sediments (Fig. 7b). In addition, the pronounced LREE depletion observed for the Siberian traps and the Khatanga river SPM suggests that the Siberian traps do not contribute significantly to the sediment composition of the Mendeleev Ridge in the Central Arctic Ocean (see Fig. 4, data in Supplementary material). Eolian supply from the Kamchatka and the Aleutian Arc is unlikely because of their strong LREE depletion (Fig. 4). The Okhotsh-Chukotka spidergram pattern, with Ba and Nb–Ta depletion and LREE, Th, U and Pb enrichments, mimics the patterns of the MC12 sediment samples (see upper panel in Fig. 4). Finally due to its location, the weathering of the Okhotsh-Chukotka province delivers particle material to the East Siberian Sea through the drainage of Siberian rivers like Kolyma, Indigirka (Fig. 6). Such provenance is in agreement with the mineral assemblage (i.e., trace of amphibole in sand and/or coarse silt fraction, and smectite-poor clay fraction). It is notable that the average εNd signal of the Siberian river estuaries may not be used to discriminate the supplies from the Lena and the Indigirka (Guo et al., 2004) and we do not find any trace element composition of those rivers in literature (only major element data in Hugh et al., 1998; trace metal elements in Guo et al., 2004).

5.3. Evolution of sedimentary supplies over time

We interpret the changes in Nd and Pb isotope signatures (Fig. 5) in the different MIS by changes in the relative contribution of three main sources in the sedimentary mixing supplied to the Mendeleev Ridge. Since 3 end-members are identified (SPM MacKenzie, SPM Lena/Siberian craton, Okhotsh-Chukotka province), we then estimate their relative contributions within the sedimentary mixings. A mixing grid was calculated based on the mean Pb and Nd contents, $^{207}Pb/^{206}Pb$ and $^{143}Nd/^{144}Nd$ compositions of the end-members (Fig. 8). For each grid point we calculate the $^{207}Pb/^{206}Pb$ and $^{143}Nd/^{144}Nd$ of the mixing for a given contribution of the 3 end-members (Faure, 1986). In fine sediment fraction of 12MC core (Fig. 8) the contribution from MacKenzie that represents the supplies from the North American and/or the Canadian margin ranges between 25 and 70%. The lowest contributions characterise the two

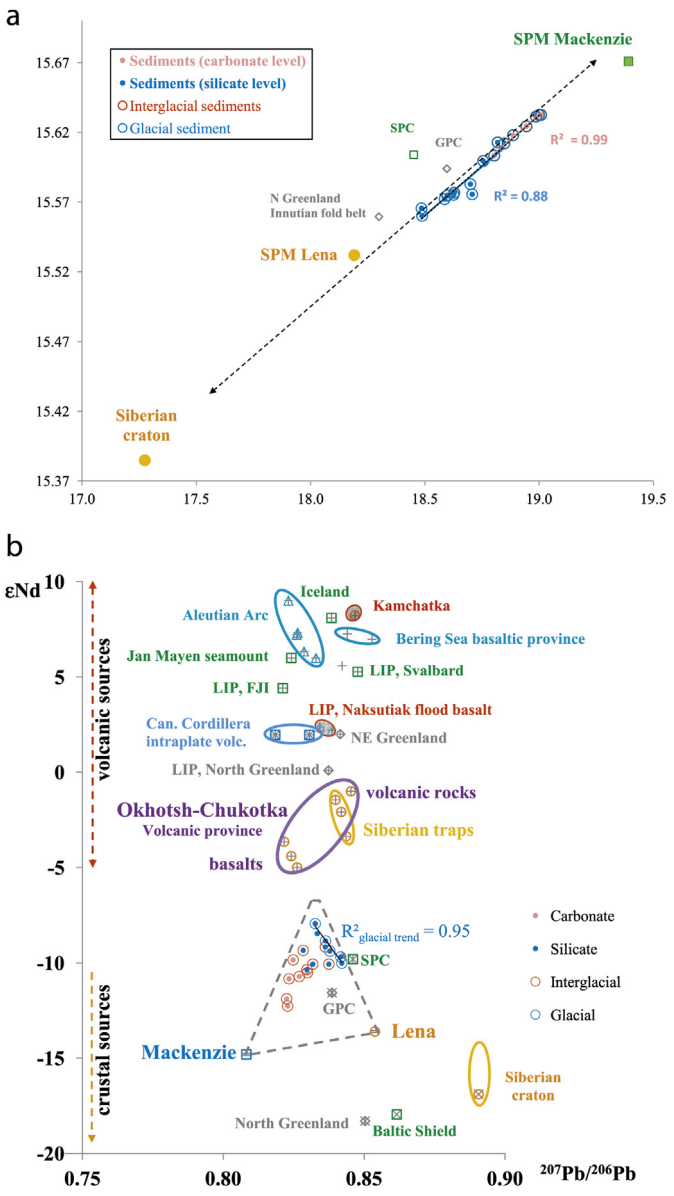

Fig. 7. aBiplot $^{207}Pb/^{206}Pb$ versus $^{208}Pb/^{206}Pb$ measured on fine <20 μm calcite-free sedimentary fraction of 12MC core by MC–ICP-MS. All samples define a linear trend (0.88 in silicate layers < r^2 < 0.99 in carbonate layers). The carbonate-rich samples (pink dot) systematically display lower Pb ratios. The silicate-rich samples are more scattered, they usually represent higher Pb ratios. The isotopic signature of regional sources is also plotted (data from Table 3). The sediment composition may be explained by a two-end-member mixing between the two Arctic margins. The MacKenzie SPM signature represents the supplies from the American margin; they dominate the sedimentary mixing in carbonate-rich 12MC samples. The Lena SPM signature represents the supplies from the Siberian margin, being more important in the silicate-rich samples. Note the representative signature of the Siberian craton also fits with the observed mixing line. b. Biplot εNd versus $^{207}Pb/^{206}Pb$ ratios measured on fine <20 μm calcite-free sedimentary fraction of 12MC core by MC-ICP-MS. The same symbols as in Fig. 7a are used: pink dot = carbonate-rich sample; blue dot = silicate-rich sample. Open red circle: interglacial samples; open blue circle: glacial samples. We report the minimum, maximum and/or the mean values for regional sources. Data from GEOROC (2003) database and from literature are listed in Table 3.

glacial stages MIS4 and MIS6. The interglacial/deglacial periods MIS1–3, 5/TII and 7/TIII are characterised by at least 50% of supplies from MacKenzie, with the highest contribution observed during MIS1–3 (~70%). The volcanic supplies contribute between 20 and 55% of the mixing. Its contribution remains stable (30–40%) from MIS7/TIII to MIS5/TII, it reaches a maximum during MIS4 then decreases towards the surface (20–30%). The Lena contribution represents a Eurasian margin supply, mainly from the Laptev Sea. It is low during MIS7/TIII (10–20%), reaches up to 40% during MIS6 and then decreases towards the surface.

5.4. Implication for the circulation of the Arctic Ocean

Sediment distribution from continental margins through the Arctic Ocean is mainly due to sea-ice and icebergs, with pathways defined by surface currents (Pfirman et al., 1997). In deep Arctic waters, sea-ice is probably the most important sediment carrier (Eicken et al., 2005; Schmitt, 2007), especially for clays and silts (Wollenburg, 1993; Dethleff, 2005). Stein (2008) estimated that 85% of the sediment on the Central Arctic ridge is supplied by sea-ice. However, glacial flour from meltwater events from ice-sheet margins can also be responsible for the transport of fine particles. Even if Arctic rivers transport large amounts of dissolved and particulate material onto the shelves, these materials are further transported by sea ice, icebergs and turbidity currents towards the open ocean. Thus, fine grain size material with a fluvial signature contributes a major proportion to the entire Arctic Ocean sediment. Finally, fine grained particles may be transported by wind into the Arctic Ocean, but the proportion of the eolian derived sediment to the Central Ocean has been shown to be very limited (Stein, 2008). In core 12MC, 60–80% of the sediment, corresponds to the size fraction <20 μm, which suggests that sea-ice is one of the main transport agents for the sediment at these sites. Dolomite clasts, sandy layers and occurrence of amphibole attest that icebergs can also play a role in sediment transport. However the fine mean grain size of core 12MC rules out any major contribution. Sea ice can incorporate sediment following two entrainment processes known as frazil ice and anchor ice. However anchor ice entrainment can be recognized in dirty ice by the presence of benthic shells or other particles much larger than 30–60 μm (Darby et al., 2011). Then the mean grain size of sediment from core 12MC suggests that frazil ice is the main transport agent for the sediment from the Central Arctic Ocean.

Since we analysed the smallest size fraction (<20 μm), which is mainly transported by sea-ice and wind, we can not discuss the IRD origin and ice-sheet evolution. Using Nd and Pb isotope signatures of the <20 μm sediment, we proposed that this fraction has three different and well define sources that reach the Northern Mendeleev Ridge. The three sediment sources, SPM from the MacKenzie river, SPM from the Lena river/Siberian craton, Okhotsh-Chukotka province, are the same during past 250 ka. Only the proportion of each source changes over time, according to glacial/interglacial variability. During MIS1–3/TI, MIS5/TII and MIS7/TIII the proportion of each source is generally constant, however the two glacial periods MIS4 and MIS6 present different sedimentary mixing between each other and during interglacial/deglacial periods.

MIS7/TIII and MIS5/TII sediments are characterised by similar mixings (40–50% from American and Canadian margins, 30% from volcanic province, 10–20% from Eurasian margin). The MIS5/TII and MIS7/TIII, which mainly correspond to the deglacial periods are characterised by dolomite-rich samples, with a geochemical signature of the North American margin. This fine sediment supply seems to be related to meltwater events from the North American ice-sheet or SPM of the Mackenzie, and its dispersion occurs via the BG. The sedimentary contribution from volcanic province and Lena area suggest some active sea ice factory along the Eurasian margin. During deglacial and interglacial periods, the TPD contribution is diluted by the BG contribution. The more pronounced contribution from American margin during MIS1–3 (Fig. 8) suggests an unusual situation. At that time the location of the BG/TPD may be slightly different than during previous interglacials MIS5 and MIS7 in agreement with Stein et al.'s (2010a) reconstructions of the BG/TPD front.

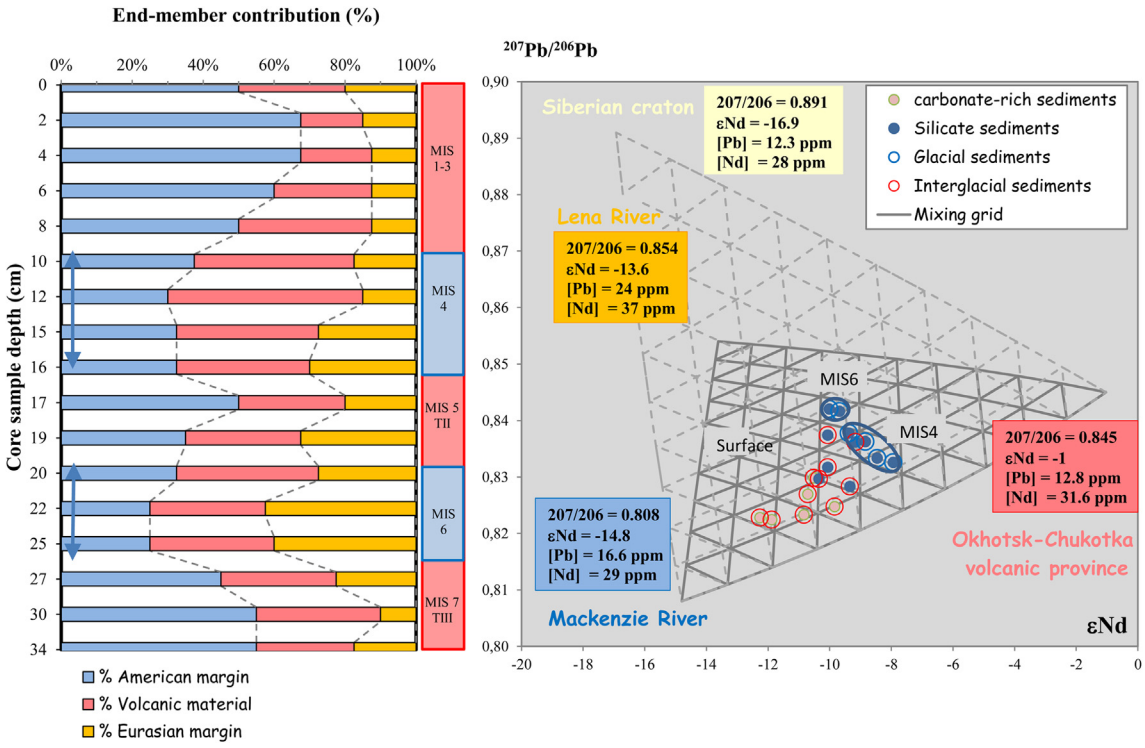

Fig. 8. Left panel. Estimated relative contribution of the three identified end-members reported versus 12MC sample depth. North American margin supplies are represented by the MacKenzie SPM signature (data from Golstein et al., 1984; Millot, 2002; Millot et al., 2004), the crustal Eurasian margin supplies by the Lena SPM signature (data from Rachold, 1999; Millot et al., 2003; Porcelli et al., 2009) and the volcanic province by the Okhotsh-Chutoka Arc (data from Porcelli et al., 2009). Mixing calculation is based on the mean [Nd], [Pb], εNd and $^{207}Pb/^{206}Pb$ ratios of the three end-members. The scale on the right gives the tentative position of the marine isotopic stages (MIS). Right panel. Ten %- increment mixing grid (plain line) used to estimate the relative contribution of the three end-members in each MC12 samples. A mixing grid taking into account the Siberian craton (data from GEOROC, 2003 database) rather than the Lena SPM is shown for comparison (dashed line). See text for further explanation.

During MIS6 a significant drop in sea level (~−90 m Rabineau et al., 2006) exposes much of the continental shelf and closes the Bering Strait, with consequence on the surface circulation (Sellen et al., 2010). The North American Ice Sheet is assumed to be as extensive as the Late Weichselian one with ice sheet margins extending as far as the Western part of the Canada Basin and in the elevated feature of the Chuckhi Sea (Jakobsson et al., 2010b). In the Eurasian margin, the extent of the Eurasian Ice Sheet is even much less constrained (see discussion in Dowdeswell et al., 2010). Based on recent studies (Colleoni et al., 2010; Stein et al., 2010a; Jakobsson et al., 2010b; Gebhardt et al., 2011) it is accepted that the Eurasian Ice Sheet extended onto Severnaya-Semlya islands and further east in the Laptev Sea. However the presence of an ice sheet in the Indigirka and its region, reaching the Arctic Ocean in the Eastern part of the Laptev sea is much more uncertain (Stein et al., 2010, Fig. 6.41). Based on the mineral assemblage and geochemical data of the 12 core, we observe limited supplies (25%) from North American margin and from the Okhotsh-Chukotka province (25%) to the sedimentary mixings, whereas approximately 50% of sediment supply comes from the Lena/Siberian craton. Such minimal contribution from the MacKenzie is consistent with the more pronounced glacial conditions on the American margin during MIS6 (Jakobsson et al., 2010b). The MacKenzie Delta is reduced or not active anymore during glacials. At that time the presence of ice shelves along the Amerasian margin limits the contribution of the Beaufort Gyre. The North American supplies are only delivered to the Central Arctic Ocean from the erosion of the Canadian Arctic Archipelago. Such supplies, probably controlled by the ice shelf extent, are evidenced by their kaolinite-rich mineral assemblage. In contrast, the East Siberian margin may remain ice sheet free even during the maximum extension of the Eurasian Ice Sheet observed during MIS6 (Svendsen et al., 2004). Siberian shelves are the main site of sea-ice production (Nürnberg et al., 1994; Dethleff, 2005; Sellen et al., 2010). According to several studies (Bischof and Darby, 1997; Krylov et al., 2008; Darby, 2008) Late Pleistocene sea ice drifting from the Siberian margin remains similar as modern TPD. Due to the absence of large ice shelves in East Siberia, particle supplies from East Siberian rivers (e.g. paleo delta for LGM in Taldenkova et al., 2010) may be incorporated in circulation, following sea ice drift (Stein et al., 2010) and explain the contribution from Okhotsh-Chukotka volcanic province.

The sediments from MIS4 are characterised by approximately 30% from the Amerasian margin, 40–55% from the Volcanic province and 15–30% from the Eurasian margin. Then the principal sediment source is the Okhotsh-Chukotka volcanic province, indicating that a supply from East Siberian rivers are incorporated and transported in sea ice. The higher proportion of the volcanic province signature can be related to an increase of this sedimentary supply or to a decrease of the two other sources in comparison to MIS6. Less is known about the ice sheet extent during the MIS4 in the Amerasian margin. In the Eurasian Basin, Svedsen et al. (1999) have published a map of maximum ice sheet extent on the Siberian shelf for MIS4. More recently the distribution of seismic units in the late Quaternary sedimentary succession along the Western Laptev Sea margin indicates the occurrence of an ice sheet grounding line near the shelf break that was attributed to a maximum Weischelian ice sheet extent during MIS4 (Kleiber et al., 2001a,b). The Eurasian Ice Sheet reached the Severnaya-Semlya islands but no sign of a further advance in the Laptev Sea like during MIS6 is observed (Svendsen et al., 2004). In addition, the sea level was higher during MIS4 (~−65 m; Kleiber et al., 2001) than during MIS6 (~−90 m; Rabineau et al., 2006). Since this change is observed in the finer size

fraction, we propose that the decrease of the sedimentary supply from the Canadian margin and from the Lena area is responsible for the change in sedimentary supply proportion between MIS6 and MIS4. The presence of larger shelves could be responsible to a more limited dispersion of the sediment in the Central Arctic Ocean.

6. Conclusion

Mineralogical, geochemical and Nd and Pb isotope data of the fine sediment fraction (<20 μm) of deep cores have enabled the identification of the main sedimentary sources delivered to the Central Arctic Ocean during the late Quaternary period. The three sediment sources, SPM from the MacKenzie river, SPM from the Lena river/Siberian craton, Okhotsh-Chukotka province, are continuously maintained during the past 250 ky. However the relative contribution of the sedimentary supplies exhibit pronounced glacial/interglacial–deglacial changes. Taking into account the actual surface current distribution, most American margin supplies are delivered to the Central Arctic Ocean by the Beaufort Gyre (BG). Assuming that all volcanic supplies originated from East Siberia are mainly delivered by rivers and then sea ice, both the volcanic and Lena contribution are delivered to the East Siberian and Laptev seas, mainly feeding the Trans Polar Drift (TPD). The evolution of sedimentary mixings may be interpreted by the relative contribution of the two main surface currents to particle delivery to the Central Arctic Ocean. Supplies from the American margin indirectly represent the main source of particle transport by the BG. Supplies from the Eurasian (East Siberia) margin reflect the main source of particle transport by the TPD. During active glacial periods, our data suggest that at least 70% of the sediment particles delivered to the Central Arctic Ocean are driven by TPD. During deglacial events, our data emphasise a dramatic reduction of the TPD contribution (down to 30%) in the sediment transport to the Northern Mendeleev Ridge.

Acknowledgements

We thank for their technical support Michel Preda for sample preparation and X-ray diffraction analyses (Geotop, Montreal), Catherine Chauvel for ICP-MS analyses (Grenoble, France) and Jeroen De Jong for MC–ICP-MS (G-Time, ULB); Romain Millot (BRGM, France) for the provision of some thesis data. English editing has been kindly done by Dr. Anson Mackay from University College of London (UCL). The authors also acknowledge the reviewers and the editor for their comments on the manuscript.

References

Aagaard, K., Swift, J.H., Carmack, E.C., 1985. Thermohaline circulation in the Arctic Mediterranean Seas. J. Geophys. Res. 90, 4833–4846.
Aagaard, K., 1989. A synthesis of the Arctic Ocean circulation. Rapp. P-V. Reun. Cons. Int. Explor. Mer. 188, 11–22.
Abouchami, W., Galer, S.J.G., Hofmann, A.W., 2000. High precision lead isotope systematics of lavas from the Hawaiian Scientific Drilling Project. Chem. Geol. 169, 187–209.
AMAP, 1998. AMAP Assessment Report: Arctic Pollution Issues. Arctic Monitoring and Assessment Programme (AMAP), Oslo, Norway.
Asahara, Y., Takeuchi, F., Nagashima, K., Harada, N., Yamamoto, K., Oguri, K., Tadai, O., 2012. Provenance of terrigenous detritus of the surface sediments in the Bering and Chukchi Seas as derived from Sr and Nd isotopes: implications for recent climate change in the Arctic regions. Deep Sea Res. II Top. Stud. Oceanogr. 61–64, 155–171.
Biscaye, P.E., 1965. Mineralogy and sedimentation of recent deep-sea clay in the Atlantic Ocean and adjacent seas and oceans. Geol. Soc. Am. Bull. 76, 803–832.
Bischof, J.F., Darby, D.A., 1997. Mid-to Late Pleistocene Ice Drift in the Western Arctic Ocean: evidence for a different circulation in the past. Science 277 (5322), 74–78.
Boski, T., Pessoa, J., Pedro, P., Thorez, J., Dias, J.M.A., Hall, I.R., 1998. Factors governing abundance of hydrolysable amino acids in the sediments from the NW European Continental margin (47–50°N). Prog. Oceanogr. 42, 145–164.
Buchan, K.L., Ernst, 2006. Giant dyke swarms and the reconstruction of the Canadian Arctic islands, Greenland, Svalbard and Franz Josef Land. In: Hanski, E., Mertanen, S., Ramo, T., Vuollo, J. (Eds.), Dyke Swarms: Time Markers of Crustal Evolution. Taylor and Francis/Balkema Publishers, London, pp. 27–48. http://www.largeigneousprovinces.org/06apr. Consulted 28/02/2012.
Chauvel, C., Blichert-Toft, J., 2001. A hafnium isotope and trace element perspective on melting of the depleted mantle. Earth Planet. Sci. Lett. 190, 137–151.
Cocks, L.R.M., Torsvik, T.H., 2007. Siberia, the wondering northern terrane, and its changing geography through the Palaeozoic. Earth Sci. Rev. 82, 29–74.
Colleoni, F., Jakobsson, M., Krinner, G., 2010. The role of the Late Saalian Arctic ice-shelf in the climate of the last glacial maximum of MIS 6 (140 ka). Quat. Sci. Rev. 29, 3590–3597.
Cook, H.E., Johnson, P.D., Matti, J.C., Zemmels, I., 1975. Methods of sample preparation and x-ray diffraction analysis in x-ray mineralogy laboratory. In: Kaneps, A.G., et al. (Eds.), Init. Repts DSDP XXVIII. Print. Office, Washington DC, pp. 997–1007.
Darby, D.A., 1975. Kaolinite and other clay minerals in Arctic Ocean sediments. J. Sed. Petrol. 45, 272–279.
Darby, D.A., Jakobsson, M., Polyak, L., 2005. Ice breaker expedition collects key Arctic seafloor and ice data. EOS Trans. AGU 86, 549–552.
Darby, D.A., Zimmerman, P., 2008. Ice-rafted detritus events in the Arctic during the Last Glacial Interval and the Timing of the Innuitian and Laurentide Ice Sheet Calving Events. Polar Res. 27, 114–127. http://dx.doi.org/10.1111/j.1751-8369.2008.00057.
Darby, D.A., Myers, W.B., Jakobsson, M., Rigor, I., 2011. Modern dirty sea ice characteristics and sources: the role of anchor ice. J. Geophys. Res. 116, C09008. http://dx.doi.org/10.1029/2010JC006675.
Dethleff, D., 2005. Entrainment and export of Laptev Sea ice sediments, Siberian Arctic. J. Geophys. Res 110, C07009. http://dx.doi.org/10.1029/2004JC002740.
Dia Hantchi, K., 2000. Géochimie isotopique Sr-Nd-Pb des sédiments accumulés depuis 700 000 ans le long de la dorsale de Reykjanes (58–60° Nord). UQAM, Montreal, Canada, p. 219 (Thèse de doctorat).
Dowdeswell, J.A., Jakobsson, M., Hogan, K.A., O'Regan, M., Backman, J., Evans, J., Hell, B., Löwemark, L., Marcussen, C., Noormets, R., Cofaigh, C.O., Sellén, E., Sölvsten, M., 2010. High-resolution geophysical observations of the Yermak Plateau and northern Svalbard margin: implications for ice-sheet grounding and deep-keeled icebergs. Quat. Sci. Rev. 29, 3518–3531. http://dx.doi.org/10.1016/j.quascirev.2010.06.002 (25–26, APEX Spec. Iss.,).
Dupuy, C., Michard, A., Dostal, J., Dautel, D., Baragar, W.R.A., 1995. Isotope and trace-element geochemistry of Proterozoic Natkusiak flood basalts from the northwestern Canadian Shield. Chem. Geol. 120 (1–2), 15–25.
Dyke, A.S., Andrews, J.T., Clark, P.U., England, J.H., Miller, G.H., Shaw, J., Veillette, J.J., 2002. The Laurentide and Innuitian ice sheets during the Last Glacial Maximum. Quat. Sci. Rev. 21 (1–3), 9–31.
Eicken, H., Gradinger, R., Gaylord, A., Mahoney, A., Rigor, I., Melling, H., 2005. Sediment transport by sea ice in the Chukchi and Beaufort Seas: increasing importance due to changing ice conditions? Deep Sea Res. II Top. Stud. Oceanogr. 52, 3281–3302.
Eisenhauer, A., Meyer, H., Rachold, V., Tütken, T., Wiegand, B., Hansen, B.T., Spielhagen, R.F., Lindemann, F., Kassens, H., 1999. Grain size separation and sediment mixing in Arctic Ocean sediments: evidence from the strontium isotope systematic. Chem. Geol. 158, 173–188.
Elverhøi, A., Rønningsland, T.M., 1978. Semiquantitative calculation of the relative amounts of kaolinite and chlorite by X-ray diffraction. Mar. Geol. 27, 19–23.
England, J.H., Furze, M.F.A., Doupe, J.P., 2009. Revision of the NW Laurentide Ice Sheet: implications for paleoclimate, the northeast extremity of Beringia, and Arctic Ocean sedimentation. Quat. Sci. Rev. 28, 1573–1596.
Fagel, N., 2007. Marine clay minerals, deep circulation and climate. In: Hillaire-Marcel, C., de Vernal, A. (Eds.), Paleoceanography of the Late Cenozoic, Methods, vol. 1. Elsevier, Amsterdam, pp. 139–184.
Fagel, N., Innocent, C., Gariepy, C., Hillaire-Marcel, C., 2002. Sources of Labrador Sea sediments since the last glacial maximum inferred from Nd–Pb isotopes. Geochim. Cosmochim. Acta 66 (14), 2569–2581.
Fagel, N., Boës, X., 2008. Clay-mineral record in Lake Baikal sediments: the Holocene and Late Glacial transition. Palaeogeogr. Palaeoclimatol. Palaeoecol. 259, 230–243.
Faure, G., 1986. Principles of Isotope Geology, second ed. John Wiley & Sons, p. 589.
Galer, S.J.G., Abouchami, W., 1998. Practical application of lead triple spiking for correction of instrumental mass discrimination. 8th Goldschmidt Conf. Mineral. Mag. 62A, 491–492.
GEOROC, 2003. Geochemistry of Rocks of the Oceans and Continents. MPI für Chemie/Max-Planck Institute fur Chemie, Mainz, Germany. Visited in March 2012. http://georoc.mpch-mainz.gwdg.de/S.
Gebhardt, A.C., Jokat, W., Niessen, F., Matthiessen, J., Geissler, W.H., Schenke, H.W., 2011. Ice sheet grounding and iceberg plow marks on the northern and central Yermak Plateau revealed by geophysical data. Quat. Sci. Rev 30, 13–14. http://dx.doi.org/10.1016/j.quascirev.2011.03.016.
Goldstein, S.L., O'Nions, R.K., Hamilton, P.J., 1984. A Sm–Nd isotopic study of atmospheric dust particulates from major river systems. Earth Planet. Sci. Lett. 70, 221–236.
Guo, L., Semiletov, I., Gustafsson, O., Ingri, J., Andersson, P., Dudarev, O., White, D., 2004. Characterization of Siberian Arctic coastal sediments: implications for terrestrial organic carbon export. Global Biogeochem. Cycles 18, GB1036. http://dx.doi.org/10.1029/2003GB002087.

Haley, B.A., Frank, M., Spielhagen, R., Fietzke, J., 2008a. Radiogenic isotope record of Arctic Ocean circulation and weathering inputs of the past 15 million years. Paleoceanography 23. http://dx.doi.org/10.1029/2007PA001486. Paper PA1S13.
Haley, B.A., Frank, M., Spielhagen, R.F., Eisenhauer, A., 2008b. Influence of brine formation on Arctic Ocean circulation over the past 15 million years. Nat. Geosci. 1, 68–72.
Haley, B.A., Polyak, L., 2013. Pre-modern Arctic Ocean circulation from surface sediment neodymium isotopes. Geophys. Res. Lett 40. http://dx.doi.org/10.1002/GRL.50188, 2013.
Harrison, J.C., St-Onge, M.R., Petrov, O., Strelnikov, S., Lopatin, B., Wilson, F., Tella, S., Paul, D., Lynds, T., Shokalsky, S., Hults, C., Bergman, S., Jepsen, H.F., Solli, A., 2008. Geological Map of the Arctic. Geol. Survey Canada, p. 5816. Open File.
Hoffman, S.S., McManus, J.F., Curry, W.B., Brown-Leger, L.S., 2013. Persistent export of ^{231}Pa from the deep central Arctic Ocean over the past 35,000 years. Nature 497, 603–607. http://dx.doi.org/10.1038/nature12145.
Huh, Y., Panteleyev, G., .Babich, D., Zaitsev, A., Edmond, J.M., 1998. The fluvial geochemistry of the rivers of Eastern Siberia: II. Tributaries of the Lena, Omoloy, Yana, Indigirka, Kolyma, and Anadyr draining the collisional/accretionary zone of the Verkhoyansk and Cherskiy ranges. Geochim. Cosmochim. Acta 62 (12), 2053–2075.
Jang, K., Han, Y., Huh, Y., Nam, S., Stein, R., Mackensen, A., Matthiessen, J., 2013. Glacial freshwater discharge events recorded by authigenic neodymium isotopes in sediments from the Mendeleev Ridge, western Arctic Ocean. Earth Planet. Sci. Lett. 369–370, 148–157.
Jakobsson, M., Lovlie, R., Al-Hanbali, H., Arnold, E., Backman, J., Mörth, M., 2000. Manganese and color cycles in Arctic Ocean Sediments constrain Pleistocene chronology. Geology 28, 23–26.
Jakobsson, M., Long, A., Ingólfsson, O., Kjær, K.H., Spielhagen, R.F., 2010a. New insights on Arctic Quaternary climate variability from palaeo-records and numerical modeling. Quat. Sci. Rev. 29, 3349–3358.
Jakobsson, M., Nilsson, J., O'Regan, M., Backman, J., Löwemark, L., Dowdeswell, J.A., Mayer, L., Polyak, L., Colleoni, F., Anderson, L., Björk, G., Darby, D., Eriksson, B., Hanslik, D., Hell, B., Marcussen, C., Sellén, E., Wallin, Å., 2010b. An Arctic Ocean ice shelf during MIS 6 constrained by new geophysical and geological data. Quat. Sci. Rev 29, 3505–3517. http://dx.doi.org/10.1016/j.quascirev.2010.03.015.
Jicha, B.R., Singer, B.S., Brophy, J.G., Fournelle, J.H., Johnson Clark, M., Beard, B., Lapen, T.J., Mahlen, N.J., 2004. Variable impact of the subducted slab on Aleutian Island Arc Magma Sources: evidence from Sr Nd Pb and Hf isotopes and trace element abundances. J. Petrol. 45, 1845–1875.
Kellogg, W.W., 1995. Contaminants affecting the Arctic climate, and the role of the oceans. Sci. Total Environ. 160–161, 769–775.
Kleiber, H.P., Niessen, F., Weiel, D., 2001a. The Late Quaternary evolution of the western Laptev Sea continental margin, Arctic Siberia – implications from sub-bottom profiling. Global Planet. Change 31, 105–124.
Kleiber, H.P., Niessen, F., Weiel, D., 2001b. The Late Quaternary evolution of the western Laptev Sea continental margin, Arctic Siberia – implications from sub-bottom profiling. Global Planet. Change 31, 105–124 (1–4 (QUEEN Special Issue)).
Krylov, A.A.., Andreeva, I.A., Vogt, C., Backman, J., Krupskaya, V.V., Grikurov, G.E., Moran, K., Shoji, H., 2008. A shift in heavy and clay mineral provenance indicates a middle Miocene onset of a perennial sea ice cover in the Arctic Ocean. Paleoceanography 23, PA1S06. http://dx.doi.org/10.1029/2007PA001497.
Maccali, J., Hillaire-Marcel, C., Carignan, J., Reisberg, L.C., 2012. Pb isotopes and geochemical monitoring of Arctic sedimentary supplies and water mass export through Fram Strait since the Last Glacial Maximum. Paleoceanography 27, PA1201. http://dx.doi.org/10.1029/2011PA002152.
McDonald, R.W., Harner, T., Fyfe, J., 2005. Recent climate change in the Arctic and its impact on contaminant pathways and interpretation of temporal trend data. Sci. Total Environ. 342, 5–86.
Martin, R.T., Bailey, S.W., Eberl, D.D., Fanning, D.S., Guggenheim, S., Kodama, H., Pevear, D.R., Środoń, J., Wicks, F.J., 1991. Report on the Clay Minerals Society nomenclature committee: revised classification of clay minerals. Clays Clay Min. 39, 333–335.
McLennan, S.M., 2001. Relationships between the trace element composition of sedimentary rocks and upper continental crust. Geochem. Geophys. Geosyst. 2 (4). http://dx.doi.org/10.1029/2000GC000109.
Martinson, D.G., Pisias, N.G., Hays, J.D., Imbrie, J., Moore Jr., T.C., Shackleton, N.J., 1987. Age dating and the orbital theory of the Ice Ages: development of a high-resolution 0–300,000 year chronostratigraphy. Quat. Res. 27, 1–29.
Millot, R., 2002. Etude Chimique et Isotopique des produits d'érosion des grands fleuves canadiens: impact des rivières boréales dans les bilans globaux d'altération (Ph. D. thesis). Université Paris 7, Denis Diderot, p. 270.
Millot, R., Gaillardet, J., Dupré, B., Allègre, C.J., 2003. Northern latitude chemical weathering rates: clues from the MacKenzie River Basin, Canada. Geochim. Cosmochim. Acta 67, 1305–1329.
Millot, R., Allègre, C.J., Gaillardet, J., Roy, S., 2004. Lead isotopic systematics of major river sediments: a new estimate of the Pb isotopic composition of the Upper Continental Crust. Chem. Geol. 203, 5–90.
Moore, D.M., Reynolds, R.C., 1997. X-ray Diffraction and the Identification and Analysis of Clay Minerals, second ed. Oxford University Press, p. 378.
Mühe, R., Bohrmann, H., Garbe-Schönberg, D., Kassens, H., 1997. E-MORB glasses from the Gakkel Ridge (Arctic Ocean) at 87.8°N: evidence for the Earth's most northerly volcanic activity. Earth Planet. Sci. Let 152, 1–9.
Not, C., Hillaire-Marcel, C., 2012. Enhanced sea-ice export from the Arctic during the Younger Dryas. Nat. Commun. 3, 647.
Not, C., Hillaire-Marcel, C., 2010. Time constraints from ^{230}Th and ^{231}Pa data in late Quaternary, low sedimentation rate sequences from the Arctic Ocean: an example from the northern Mendeleev Ridge. Quat. Sci. Rev. 29, 3665–3675.
Nürnberg, D., Wollenburg, I., Dethleff, D., Eicken, H., Kassens, H., Letzig, T., Reimnitz, E., Thiede, J., 1994. Sediments in Arctic sea ice: implications for entrainment, transport and release. Mar. Geol. 119 (3–4), 185–214.
Patchett, P.J., Embry, A.F., Ross, G.M., Beauchamp, B., Harrison, J.C., Mayr, U., Isachsen, C.E., Rosenberg, E.J., Spence, G.O., 2004. Sedimentary cover of the Canadian shield through Mesozoic time reflected by Nd isotopic and geochemical results for the Sverdrup Basin, Arctic Canada. J. Geol. 112, 39–57.
Petschick, R., Kuhn, G., Gingele, F., 1996. Clay mineral distribution in surface sediments of the South Atlantic: sources, transport, and relation to oceanography. Mar. Geol. 130, 203–229.
Pfirman, S.L., Colony, R., Nurnberg, D., Eicken, H., Rigor, I., 1997. Reconstructing the origin and trajectory of drifting Arctic sea ice. J. Geophys. Res. Oceans 102 (C6), 12575–12586.
Phillips, R.L., Grantz, A., 2001. Regional variations in provenance and abundance of ice-rafted clasts in Arctic Ocean sediments: implications for the configuration of late Quaternary oceanic and atmospheric circulation in the Arctic. Mar. Geol. 172 (1–2), 91–115.
Polyak, L., Curry, W.B., Darby, D.A., Bischof, J., Cronin, T.M., 2004. Contrasting glacial/interglacial regimes in the western Arctic Ocean as exemplified by a sedimentary record from the Mendeleev Ridge. Palaeogeogr. Palaeoclimatol. Palaeoecol. 203 (1–2), 73–93.
Polyak, L., Darby, D.A., Bischof, J.F., Jakobsson, M., 2007. Stratigraphic constraints on late Pleistocene glacial erosion and deglaciation of the Chukchi margin, Arctic Ocean. Quat. Res. 67, 234–245.
Polyak, L., Bischof, J., Ortiz, J.D., Darby, D.A., Channell, J.E.T., Xuan, C., Kaufman, D.S., Løvlie, R., Schneider, D.A., Eberl, D.D., Adler, R.E., Council, E.A., 2009. Late Quaternary stratigraphy and sedimentation patterns in the western Arctic Ocean. Global Planet. Change 68, 5–17.
Porcelli, D., Andersson, P.S., Baskaran, M., Frank, M., Björk, G., Semiletov, I., 2009. The distribution of neodymium isotopes in Arctic Ocean basins. Geochim. Cosmochim. Acta 73, 2645–2659.
Rabineau, M., Berné, S., Olivet, J.-L., Aslanian, D., Guillocheau, F., Joseph, P., 2006. Paleo sea levels reconsidered from direct observation of paleoshoreline position during Glacial Maxima (for the last 500,000 yr). Earth Planet. Sci. Lett. 252, 119–137.
Rachold, V., 1999. Major, trace and rare earth element geochemistry of suspended particulate material of east Siberian rivers draining to the Arctic Ocean. In: Kassens, H., Bauch, H.A., Dmitrenko, I.A., Eicken, H., Hubberten, H.-W., Melles, M., Thiede, J., Timokhov, L.A. (Eds.), Land-ocean Systems in the Siberian Arctic: Dynamics and History. Springer, Berlin, Heidelberg, pp. 199–222.
Revel, M., Cremer, M., Grousset, F.E., Labeyrie, L., 1996. Grain-size and Sr–Nd isotopes as tracer of paleo-bottom current strength, Northeast Atlantic Ocean. Mar. Geol. 131 (3–4), 233–249.
Rossak, B.T., Kassens, H., Lange, H., Thiede, J., 1999. Clay mineral distribution in surface sediments of the Laptev Sea: indicator for sediment provinces, dynamics and sources. In: Kassens, H., Bauch, H.A., Dmitrenko, I., Eicken, H., Hubberten, H.-W., Melles, M., Thiede, J., Timokhov, L. (Eds.), Land–Ocean Systems in the Siberian Arctic: Dynamics and History. Springer, Berlin, pp. 587–599.
Rudels, B., Anderson, L., Eriksson, P., Fahrbach, E., Jakobsson, M., Jones, E.P., Melling, H., Prinsenberg, S., Schauer, U., Yao, T., 2012. Observations in the Ocean, Arctic Climate Change. In: Lemke, P., Jacobi, H.-W. (Eds.), Arctic Climate Change: the ACSYS Decade and Beyond, Atmospheric and Oceanographic Sciences Library, V43, Part I. Springer, Netherlands, pp. 117–198. http://dx.doi.org/10.1007/978-94-007-2027-5,4.
Schlosser, P., Swift, J.H., Lewis, D., Pfirman, S.L., 1995. The role of the large-scale Arctic Ocean circulation in the transport of contaminants. Deep Sea Res. II Top. Stud. Oceanogr. 42 (6), 1341–1367.
Schmitt, W., 2007. Application of the Sm-Nd Isotope System to the Late Quaternary Paleoceanography of the Yermak Plateau (Arctic Ocean). de l'université Ludwig-Maximilians de Munich, p. 121 (Thèse de doctorat).
Schoster, F., Behrends, M., Müller, C., Stein, R., Washner, M., 2000. Modern river discharge and pathways of supplied material in the Eurasian Arctic Ocean: evidence from mineral assemblages and major and minor element distribution. Int. J. Earth Sci. 89 (3), 486–495.
Sellen, E., O'Regan, M., Jakobsson, M., 2010. Spatial and temporal Arctic Ocean depositional regimes: a key to the evolution of ice drif and current patterns. Quat. Sci. Rev. 29, 3644–3664.
Singer, B.S., Jicha, B.R., Leeman, W.P., Rogers, N.W., 2007. Along-strike trace element and isotopic variation in Aleutian Island Arc Basalt: subduction melts sediments and dehydrates serpentine. J. Geophys. Res B112 (2006JB004897).
Stein, R., 2008. Arctic Ocean sediments: processes, proxies, and palaeoenvironment. In: Developments in Marine Geology, vol. 2Elsevier, Amsterdam, p. 592.
Stein, R., Matthießen, J., Niessen, F., Krylov, A., Nam, S., Bazhenova, E., 2010. Towards a better (litho-) stratigraphy and reconstruction of Quaternary paleoenvironment in the Amerasian Basin (Arctic Ocean). Polarforschung 79 (2), 97–121.
Sun, S.S., McDonough, W.F., 1989. Chemical and isotopic systematics of oceanic basalts; implications for mantle composition and processes. In: Saunders, A.D., Norry, M.J. (Eds.), Magmatism in the Ocean Basins, vol. 42Geol. Soc. London, London, pp. 313–345.
Svendsen, J.I., Astakhov, V.I., Bolshiyanov, D.Y., Demidov, I., Dowdeswell, Gataullin, V., Hjort, C., Hubberten, H.W., Larsen, E., Mangerud, J., Melles, M., Möller, P., Saarnisto, M., Siegert, 1999. Maximum extent of the Eurasian ice

sheet in the Barents and Kara Sea region during the Wzeischelian. Boreas 28, 234–242.
Svendsen, J.I., Alexanderson, H., Astakhov, V.I., Demidov, I., Dowdeswell, J.A., Funder, S., Gataullin, V., Henriksen, M., Hjort, C., Houmark-Nielsen, M., Hubberten, H.W., Ingólfsson, Ó., Jakobsson, M., Kjær, K., Larsen, E., Lokrants, H., Lunkka, J.P., Lysså, A., Mangerud, J., Matiouchkov, A., Murray, A., Möller, P., Niessen, F., Nikolskaya, O., Polyak, L., Saarnisto, M., Siegert, C., Siegert, M.J., Spielhagen, R.F., Stein, R., 2004. Late Quaternary ice sheet history of eastern Eurasia. Quat. Sci. Rev. 23, 1229–1271.
Taldenkova, E., Bauch, H.A., Gottschalk, J., Nikolaev, S., Rostovtseva, Y., Pogodina, I., Ovsepyan, Y., Kandiano, E., 2010. History of ice-rafting and water mass evolution at the northern Siberian continental margin (Laptev Sea) during Late Glacial and Holocene times. Quat. Sci. Rev. 29, 3919–3935.
Tikhomirov, P.L., Kalinina, E.A., Kobayashi, K., Nakamura, E., 2008. Late Mesozoic silicic magmatism of the North Chukotka area (NE Russia): age, magma sources, and geodynamic implications. Lithos 105, 329–346.
Tütcken, T., Eisenhauer, A., Wiegand, B., Hansen, B.T., 2002. Glacial–interglacial cycles in Sr and Nd isotopic composition of Arctic marine sediments triggered by the Svalbard/Barents Sea ice sheet. Mar. Geol. 182 (3–4), 351–372.
Viscosi-Shirley, C., Mammone, K., Pisias, N., Dymond, J., 2003. Clay mineralogy and multi-element chemistry of surface sediments on the Siberian-Arctic shelf: implications for sediment provenance and grain size sorting. Contin. Shelf Res. 23 (11–13), 1175–1200.
Vogt, C., Knies, J., 2008. Sediment dynamics in the Eurasian Arctic Ocean during the last deglaciation – the clay mineral group smectite perspective. Mar. Geol. 250, 211–222.
Vogt, C., Knies, J., Spielhagen, R.F., Stein, R., 2001. Detailed mineralogical evidence for two nearly identical glacial/deglacial cycles and Atlantic water advection to the Arctic Ocean during the last 90,000 years. Global Planet. Change 31 (1–4), 23–44.
Wahsner, M., Müller, C., Stein, R., Ivanov, G., Levitan, M., Shelekhova, E., Tarasov, G., 1999. Clay-mineral distribution in surface sediments of the Eurasian Arctic Ocean and continental margin as indicator for source areas and transport pathways a synthesis. Boreas 28, 215.
Wasserburg, G.J., Jacobsen, S.B., De Paolo, D.J., McCulloch, M.T., Wen, T., 1981. Precise determination of Sm/Nd ratios, Sm and Nd isotopic abundances in standard solutions. Geochim. Cosmochim. Acta 45, 2311–2323.
Weis, D., Kieffer, B., Maerschalk, C., Barling, J., de Jong, J., Williams, G.A., Hanano, D., Pretorius, W., Mattielli, N., Scoates, J.S., Goolaerts, A., Friedman, R.M., Mahoney, J.B., 2006. High-precision isotopic characterization of USGS reference materials by TIMS and MC–ICP-MS. Geochem. Geophys. Geosyst. 7.
Winter, B.L., Johnson, C.M., Clark, D.L., 1997. Strontium, neodymium, and lead isotope variations of authigenic and silicate sediment components from the Late Cenozoic Arctic Ocean: implications for sediment provenance and the source of trace metals in seawater. Geochim. Cosmochim. Acta 61, 4181–4200.
Wollenburg, I., 1993. Sediment transport durch das arktische Meereis: die rezente lithogene and biogene Materialfracht. Ber Polarforsch 127, 159.
Wooden, J.L., Czamanske, D.K., Fedorenko, V.A., Arndt, Chauvel C., Bouse, R.M., King, B.W., Knight, R.J., Siem, D.F., 1993. Isotopic and trace-element constraints on mantle and crustal contributions to Siberian continental flood basalts, Noril'sk area, Siberia. Geochim. Cosmochim. Acta 57 (19), 3677–3704.
Zimmermann, B., Porcelli, D., Frank, M., Andersson, P.S., Baskaran, M., Lee, D.-C., Halliday, A.N., 2009. Hafnium isotopes in Arctic Ocean water. Geochim. Cosmochim. Acta 73, 3218–3233.